nature communications

Article

https://doi.org/10.1038/s41467-025-67132-6

A corticospinal signature for interindividual pain sensitivity

Received: 27 August 2025

Accepted: 24 November 2025

Published online: 11 December 2025

Check for updates

Xiao-Min Lin[1,2], Ling-Fei Guo[3] ✉, Bing Ni[4] ✉, Jiu-Quan Zhang[5] ✉, Xiao-Shuo Zhang[1,2], Li-Bo Zhang[1,2,6], Zhao-Xing Wei[1,2,6], Yun-Yun Duan[7], Li Hu[1,2], Ming Zhang[1,2], Jing-Yi Zhang[1,2], Min Shao[1,2], Zai-Ying Jiang[4], Yun-Jian Huang[4], Ji-Xin Liu[8], Li-Ming Cheng[9], Jonathan C. W. Brooks[10], Tor D. Wager[6], Irene Tracey[11], Ya-Ou Liu[7] ✉ & Ya-Zhuo Kong[1,2,11] ✉

Pain sensitivity variations represent a critical frontier in pain neuroscience, where advanced neuroimaging has mapped cerebral correlates of nociception for decades, yet conventional brain-centric models persistently overlook the spinal cord's hub role in pain gating and amplification. Here we show that a corticospinal pain sensitivity signature, a pattern of functional connectivity from simultaneous corticospinal magnetic resonance imaging, predicts individual pain sensitivity and clinical pain. Trained on resting-state data and validated across independent healthy (n = 723) and patient cohorts (n = 46), the model generalized to new datasets, distinguished pain from non-pain, and outperformed brain-centric models. Crucially, transcranial magnetic stimulation perturbation revealed a causal axis where enhanced motor cortex-spinal connectivity directly changes pain perception (r = 0.55). These results indicate a previously unknown corticospinal biomarker that bridges laboratory pain measures and patient symptoms, providing insights into translating pain mechanisms from healthy individuals to clinical populations and informing neuromodulation approaches.

Chronic pain exerts a substantial negative impact on an individual's quality of life[1]. However, pain presents significant challenges for both basic research and clinical practice because it is highly subjective and individuals vary profoundly in their sensitivity to pain[2]. Pain sensitivity connects the two challenges in basic science and clinical practice. To successfully treat chronic pain, it is imperative to understand why only a minority of individuals develop chronic pain following injury or illness, whereas the majority recover without lasting pain[3]. Identifying neural signatures of pain sensitivity thus has theoretical and clinical importance.

Previous pain neuroimaging studies have primarily aimed to identify the neural correlates of pain perception and sensitivity, with key work by Wager et al.[4] and Rogachov et al.[5] uncovering brain regions and networks linked to acute pain and individual pain sensitivity. Importantly, several of the regions (e.g., anterior insula, mid-cingulate) emphasized in these studies also participate in

[1]State Key Laboratory of Cognitive Science and Mental Health, Institute of Psychology, Chinese Academy of Sciences, Beijing, China. [2]Department of Psychology, University of Chinese Academy of Sciences, Beijing, China. [3]Key Laboratory of Endocrine Glucose & Lipids Metabolism and Brain Aging, Ministry of Education, Department of Radiology, Shandong Provincial Hospital Affiliated to Shandong First Medical University, Jinan, Shandong, China. [4]Functional neurosurgery Department, Xuanwu Hospital, Capital Medical University, Beijing, China. [5]Department of Radiology, Chongqing University Cancer Hospital, Chongqing, China. [6]Department of Psychological and Brain Sciences, Dartmouth College, Hanover, NH, USA. [7]Department of Radiology, Beijing Tiantan Hospital, Capital Medical University, Beijing, China. [8]Center for Brain Imaging, School of Life Science and Technology, Xidian University, Xi'an, China. [9]Key Laboratory of Spine and Spinal Cord Injury Repair and Regeneration, Tongji University, Ministry of Education, Shanghai, China. [10]Institute of Population Health, University of Liverpool, Liverpool, UK. [11]Wellcome Centre for Integrative Neuroimaging, FMRIB, Nuffield Department of Clinical Neurosciences, University of Oxford, Oxford, UK. ✉e-mail: glfsci@163.com; nibing@xwh.ccmu.edu.cn; zhangjq_radiol@foxmail.com; liuyaou@bjtth.org; kongyz@psych.ac.cn

domain-general salience and attentional networks and are therefore not selective for pain per se[6]. Rather than weakening their relevance, this overlap suggests that stable, trait-like properties of these systems, such as their intrinsic coupling, may contribute to inter-individual differences in pain sensitivity. Notably, patterns in the brain's resting-state have been shown to mirror those during active tasks, and predict behavioral outcomes beyond what is captured in MRI scans[7]. These findings suggest a stable neural architecture in the resting brain that supports both cognitive and sensory functions, including those related to pain[8,9]. Recent work has also identified distinct resting-state connectivity patterns predictive of pain sensitivity, demonstrating the potential of connectome-based models for prediction[8]. While resting-state fMRI offers a more accessible clinical tool than task-based paradigms, its potential for predicting chronic pain in patients remains largely unexplored, highlighting a critical gap in applying neuroscientific insights to clinical practice.

Critically, the spinal cord's pivotal role in pain transmission and modulation has been largely overlooked. In fact, resting-state work demonstrates robust, reproducible spinal cord networks and coordinated brain–brainstem–spinal connectivity at rest[10–12]. During noxious stimulation and cognitive modulation, brainstem–spinal imaging shows somatotopic dorsal-horn responses and brainstem–spinal interactions consistent with descending control[13]. Moreover, in chronic pain, brainstem/spinal alterations are observed during both anticipation and pain, underscoring the clinical relevance of these regions[14]. Recent advances in corticospinal fMRI enable simultaneous examination of brain and cervical spinal cord activities[11,15]. While technically feasible, these measurements are challenging because the cord's small cross-section and adjacency to vertebral bone produce pronounced B0 inhomogeneity and gradient-echo EPI distortions, and because cord motion is strongly influenced by cardiac and respiratory pulsatility. Recent developments, including slice-specific/dynamic z-shimming and reduced-FOV EPI, substantially mitigate susceptibility artifacts, and physiological-noise modeling and gating strategies address pulsatile motion; standardized brainstem–cord templates further support robust joint registration[12,16–21]. Existing corticospinal research has focused on nocebo hyperalgesia and resting-state networks, encompassing classic pain-related regions from cortical areas and subcortical nuclei, such as the periaqueductal gray matter (PAG) of the brainstem, to the gray matter horns of the spinal cord. This integrated approach highlights the mechanisms by which the spinal cord participates in sensory perception and cognitive processing, aligning with recent animal studies that underscore the contributions of spinal motor circuits to memory retention[22], thereby challenging the traditional view of the spinal cord as merely a conduit for sensory transmission. However, currently, no study has integrated corticospinal patterns as a whole to identify pain-specific neural circuits, predict individual pain sensitivity, and quantify the importance of corticospinal interactions in this process.

Past research has established a strong link between pain sensitivity and clinical pain[23–26], elucidating potential predispositions to chronic pain vulnerability[24]. High pain sensitivity has been shown to be predictive of development of chronic pain[25–27] and effectiveness of chronic migraine treatment[28]. Individual sensitivity has been partly attributed to genetic factors, with studies identifying specific gene variants that modulate nociceptive processing[29]. In addition, mice with low pain sensitivity under healthy conditions demonstrated enhanced analgesic response[30] and transient nociception to cancer pain post-tumor induction, which was modulated by the opioid antagonist naltrexone. In contrast, those with high sensitivity showed serious nociception and lacked the modulation[31]. However, current literature lacks a direct connection between pain-free intrinsic neural networks and clinical pain, especially in relation to broader pain pathways. Given the spinal cord's important role in pain processing, neural signatures combining this region may offer more predictive and clinically relevant insights than brain-based models.

To address these issues, we developed a corticospinal machine learning model to predict individual differences in pain sensitivity more accurately than brain-only models, aiming for clinical applicability. We applied a predictive modeling approach based on corticospinal resting-state functional networks across eight datasets to answer key questions: (1) Can a corticospinal pain sensitivity model generalize across independent datasets? (2) Which functional connections within the corticospinal network significantly predict pain sensitivity and are pain-specific? (3) Does the corticospinal model outperform brain-only or spinal cord-only models? (4) Can the corticospinal model predict clinical pain?

Results

We computed resting-state functional connectivity using partial correlations across 139 corticospinal regions and used these features to predict pain sensitivity and clinical pain scores across six healthy and two patient datasets (see Fig. 1 and Supplementary Data 1 for details). In Dataset 1, we developed the corticospinal pain sensitivity signature (CSps) model using elastic network regression models to predict thermal pain thresholds, which successfully generalized to external datasets (2 and 3) and classified pain sensations in Dataset 4. CSps also predicted clinical pain in diabetic and zoster-associated pain patients (Datasets 5 and 6). Comparison with seven alternative models confirmed CSps's superior predictive performance. Finally, we explored the potential application and causality of CSps in neuromodulation using a sham-controlled TMS dataset, providing further insights into its therapeutic implications.

Development of the corticospinal pain sensitivity signature

The CSps was based on resting-state partial functional connectivity between the brain and cervical spinal cord. Using established brain and spinal cord atlases (see "Methods"), the preprocessed corticospinal resting-state fMRI data were segmented into 139 regions. Pain sensitivity was quantified based on thermal thresholds from a quantitative sensory testing (QST) protocol, with outliers removed. A machine learning pipeline incorporating feature normalization, selection, and elastic network regression models was employed to predict individual thermal pain sensitivity scores. Model optimization included grid search for parameter tuning and leave-one-out cross-validation (LOOCV), targeting minimization of the mean absolute error (MAE). The final optimized model was designated as the CSps (Fig. 1b).

In Dataset 1 ($n = 54$, after exclusion), normalized thermal pain threshold scores ranged from − 2.13 to 1.90, with a robust range of 3.04 (the range between the 5th and 95th percentiles). The CSps demonstrated robust predictive accuracy, achieving a Pearson correlation of 0.71 ($p < 0.0001$) between actual and predicted scores (Fig. 2a), an explained variance of 44%, and an MAE of 0.57 ($p = 0.001$).

External validation of the CSps

To validate the CSps model externally, we tested it on a test-retest dataset (Dataset 2, $n = 35$). All participants in Dataset 2 also took part in an unpublished study on the test-retest reliability of corticospinal networks over two weeks. Their baseline data, from Dataset 1, was used in the CSps training set, while Dataset 2 contains their follow-up data. After standardizing the sensitivity measurements from Dataset 2 using the mean and standard deviation from Dataset 1, thermal pain thresholds ranged from − 1.76 to 1.33, with a robust range of 2.60. The CSps model showed high predictive accuracy (Fig. 2b), with a Pearson correlation of 0.52 ($p = 0.001$), explaining 27% of the variance, and an MAE of 0.62. For further assessment of generalizability, we analyzed a third independent dataset (Dataset 3, $n = 36$, after exclusion) not included in model training or validation. The thermal pain thresholds

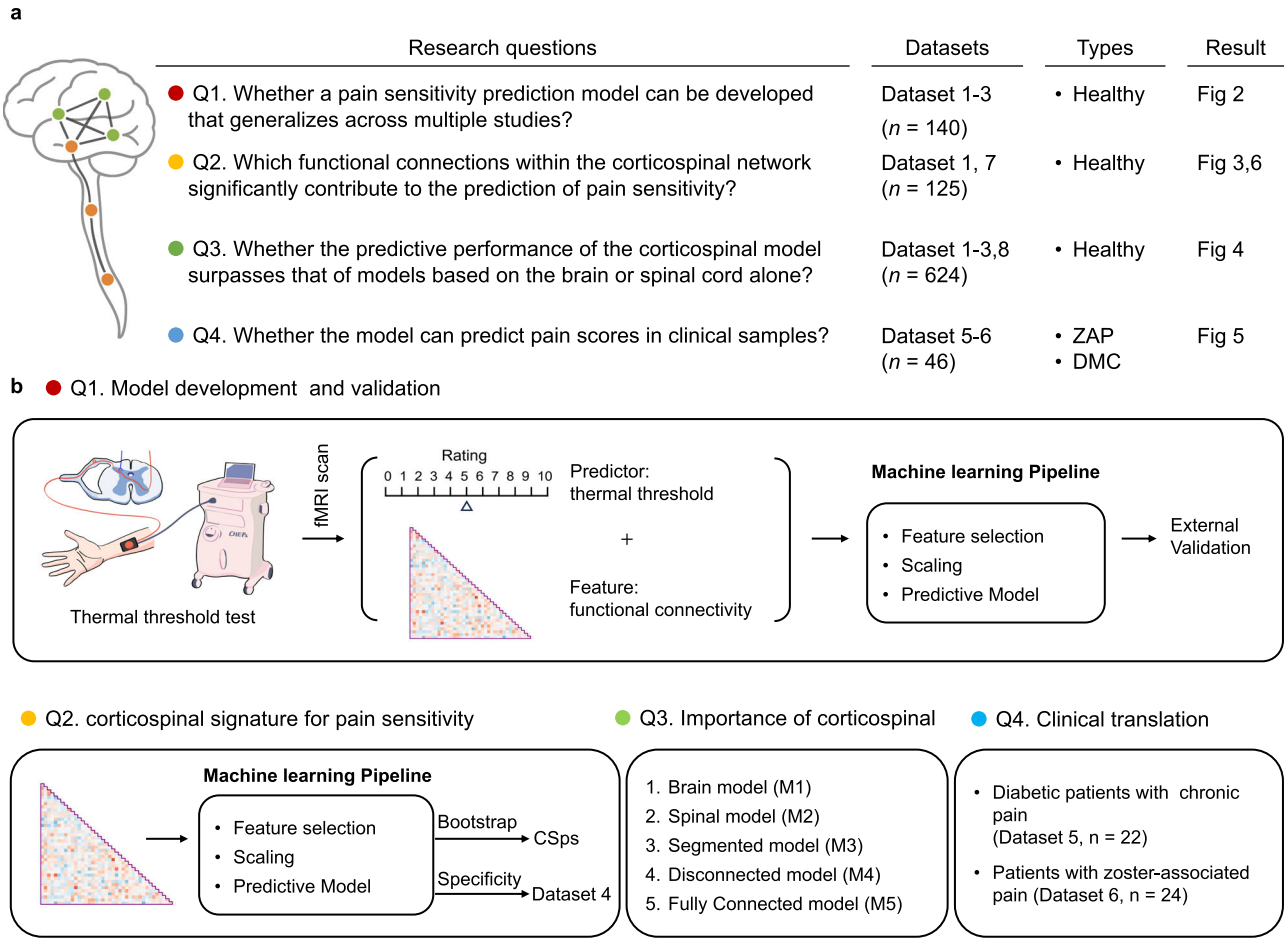

Fig. 1 | Schematic representation of the research questions and the corticospinal analysis pipeline. a This study aimed to answer four research questions (Q1-4) using six healthy and two clinical datasets. **b** the methods used include corticospinal fMRI preprocessing and predictive modeling. First, comprehensive resting-state fMRI preprocessing was performed on all subjects. Time series were then extracted for 122 brain regions using the MIST atlas registered to individual spaces. Time series of the PAG, the RVM, the dorsal and ventral horns of cervical segments C1 to C7, and the average gray matter were also included, resulting in 139 regions. Functional connectivity was computed across all regions using partial correlation, which better captures the functional relationships between nodes. The vectorized functional connectivity was used as input for predictive modeling of pain sensitivity, which was optimized via grid search for hyperparameters. The optimal model was validated on other datasets. Abbreviations: *MIST* Multi-resolution Intrinsic Segmentation Template; *PAG* periaqueductal gray; *RVM* rostroventral medulla.

ranged from −1.49 to 1.54, with a robust range of 2.65. The CSps demonstrated excellent predictive performance in Dataset 3 (Fig. 2c), with a Pearson correlation of 0.45 ($p = 0.006$), explaining 18% of the variance, and an MAE of 0.63.

Then, we tested whether our choice of a linear, regularized model constrained performance. Using the identical feature space and the same preprocessing and data splits, we re-trained two nonlinear models on Training Dataset 1: (i) support vector regression with an RBF kernel and (ii) a random-forest regressor and evaluated both models out-of-sample on Validation Datasets 2 and 3 using the study's primary metrics (Pearson r and MAE). Neither nonlinear model improved upon the elastic-net baseline (SVR: Dataset 2 $r = 0.42$, MAE = 0.72; Dataset 3 $r = 0.27$, MAE = 0.77; Random Forest: Dataset 2 $r = 0.32$, MAE = 0.70; Dataset 3 $r = 0.28$, MAE = 0.68). These findings indicate that, in our setting, a linear regularized model affords competitive out-of-sample accuracy while preserving coefficient-level interpretability. Full comparative scatterplots are provided in Supplementary Fig. S1.

Pain specificity of the CSps

To evaluate the specificity of the CSps for pain sensitivity, we conducted analyses to assess the impact of potential confounding variables, including demographic factors (age, gender, weight, height) and pain-related psychological traits (Pain Catastrophizing Scale, Pain Sensitivity Questionnaire). We tested the relationship between the predicted pain sensitivity scores and these factors using permutation-based Pearson correlations. As shown in Fig. 2d, there was no significant correlation between the model's predictions and any demographic or psychological factors (Supplementary Data 2). Overall, the CSps was unlikely to be confounded by these demographic and psychological factors.

To further assess specificity to pain, we compared the CSps response between pain and non-pain sensory conditions using a task-based dataset (Dataset 4, $n = 38$, after exclusion). By calculating dynamic conditional correlations (DCC) across 139 regions in the corticospinal pathway[9,32], we compared responses to heat pain and cold sensation (25 °C). The CSps discriminated between heat pain and cold sensation with 74% classification accuracy ($p = 0.005$), confirming its specificity for pain (Fig. 2e).

Predictive weight interpretation of the CSps

The CSps architecture is defined by a sparse set of 29 functional connections, divided into 16 positive and 13 negative weights (Supplementary Data 3). As illustrated in Fig. 3a–c, this weighting structure

https://doi.org/10.1038/s41467-025-67132-6

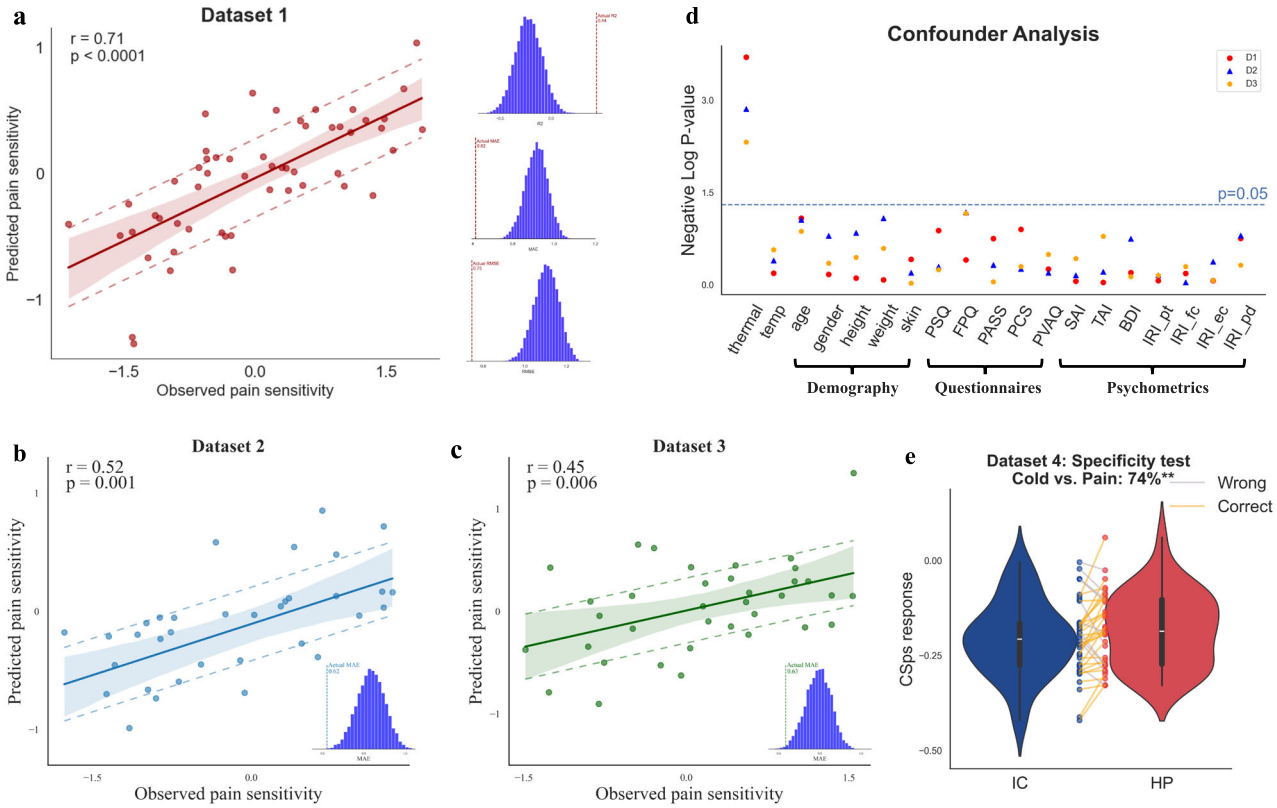

Fig. 2 | Training, external validation, confounder checks, and pain-specificity of the CSps. a Model development (Dataset 1). The CSps was trained on corticospinal resting-state functional connectivity from Dataset 1 ($n = 54$ after exclusions) using MAE as the objective, with hyperparameters optimized via grid search and leave-one-out cross-validation (LOOCV). The final setting ($K = 2000$, l1_ratio = 0.999, α = 0.1) is shown alongside the training fit. Model–outcome association: Pearson's $r = 0.71$ (two-sided $p = 1.97e\text{-}9$; 95% CI 0.589-0.802), and MAE = 0.57. The solid line is the least-squares fit; the shaded band shows the 95% CI around the fit; the measure of center is the fitted mean; dashed lines indicate the MAE. **b**, **c** External validation (Datasets 2–3). The trained CSps was applied without refitting to two independent datasets ($n = 35$ and $n = 36$ after exclusions). For Dataset 2, Pearson's $r = 0.52$ (two-sided $p = 0.001$; 95% CI 0.327-0.715), and MAE = 0.62; For Dataset 3, Pearson's $r = 0.45$ (two-sided $p = 0.006$; 95% CI 0.138-0.682), and MAE = 0.63. Insets show permutation-based MAE null distributions; reported r and p-values are permutation-derived. Dashed lines mark the observed MAE. The regression line shows the fitted mean, and the shaded band the 95% CI. No adjustment was applied across datasets. **d** Confounder analysis (Datasets 1–3). Permutation-based negative log p-values between CSps predictions and putative confounders are displayed on the y-axis. Variables include environmental temperature ("temp"), demographic factors (e.g., age, gender), pain questionnaires (e.g., PSQ, PCS), and psychometrics (e.g., STAI, BDI-II). Horizontal dashed lines mark $p = 0.05$ for the corresponding sample sizes. Two-sided permutation tests (10,000 shuffles) were used for all covariate checks. To address multiplicity across covariates within each dataset, P-values were adjusted using the FDR. Unadjusted P and adjusted q values are reported in Supplementary Data 2; no covariate survived FDR at $q < 0.05$. For transparency, the plot shows unadjusted −log10(P); the dashed line marks $p = 0.05$. **e** Specificity test (Dataset 4). A two-alternative forced-choice test contrasts average CSps responses during 25 °C innocuous cold sensation versus noxious heat. Violin plots show the distribution per condition with box-plot overlays (center line = median; box = IQR; whiskers = 1.5 × IQR; outliers shown as points). Thin connectors link each participant's paired observations. n = 38 independent participants (biological replicates); each participant contributed one paired measurement (IC vs HP). Two-alternative forced-choice accuracy = 74% with P = 0.005 (two-sided binomial test), 95% CI for accuracy = [0.58,0.85]. Abbreviations. CSps, corticospinal pain signature; MAE, mean absolute error; PSQ, Pain Sensitivity Questionnaire; PCS, Pain Catastrophizing Scale; STAI, State–Trait Anxiety Inventory; BDI-II, Beck Depression Inventory-II; IC, innocuous cold sensation; HP, heat pain. Panels are arranged by analysis type (**a**, **d**, **b**, **c**, **e**). Source data are provided as a Source Data file.

indicates that strengthened connectivity within specific edges is predictive of heightened pain sensitivity. Notably, the model's predictive capacity is concentrated; ~50% of the variance in sensitivity scores is explained by the six most robust connections. The primary positive predictor establishes a vertical axis of integration between the brain and spinal cord, specifically linking the anteromedial somatomotor network (M1 and SMA) with the C4 ventral horn. A second critical positive link connects the right dorsolateral somatomotor network to the left posterorostral middle frontal gyrus. In contrast, features predicting lower pain sensitivity (negative weights) involve distinct cortical and subcortical loops, including coupling between the ventral precuneus and lateral frontal pole, the posterior cingulate cortex and rostral inferior frontal gyrus, and bilateral hippocampal connections to the cerebellar vermis and Lobule IV.

Importance of corticospinal connection features to CSps

To assess the extent to which CSps performance depends on intra-brain, intra-spinal, or corticospinal connectivity, we trained five additional models using Dataset 1. Model M1, the Brain Model, utilized only brain connectivity features (Fig. 4a); Model M2, the Spinal Model, included only spinal cord connectivity features (Fig. 4b); Model M3, the Segmented Model, combined features from both M1 and M2 (Fig. 4c); Model M4, the Disconnection Model, excluded all corticospinal connections (Fig. 4d); and Model M5, the Solely-connected Model, incorporated only corticospinal connections (Fig. 4e). Employing the same machine learning pipeline as for CSps, we compared their performance to the original model (see "Methods"). The weighted mean explained variances across Datasets 2, 3 for CSps, M1, M2, M3, M4, and M5 were 22%, 3%, 0%, 2%, 9%, and 4%, respectively. These findings

https://doi.org/10.1038/s41467-025-67132-6

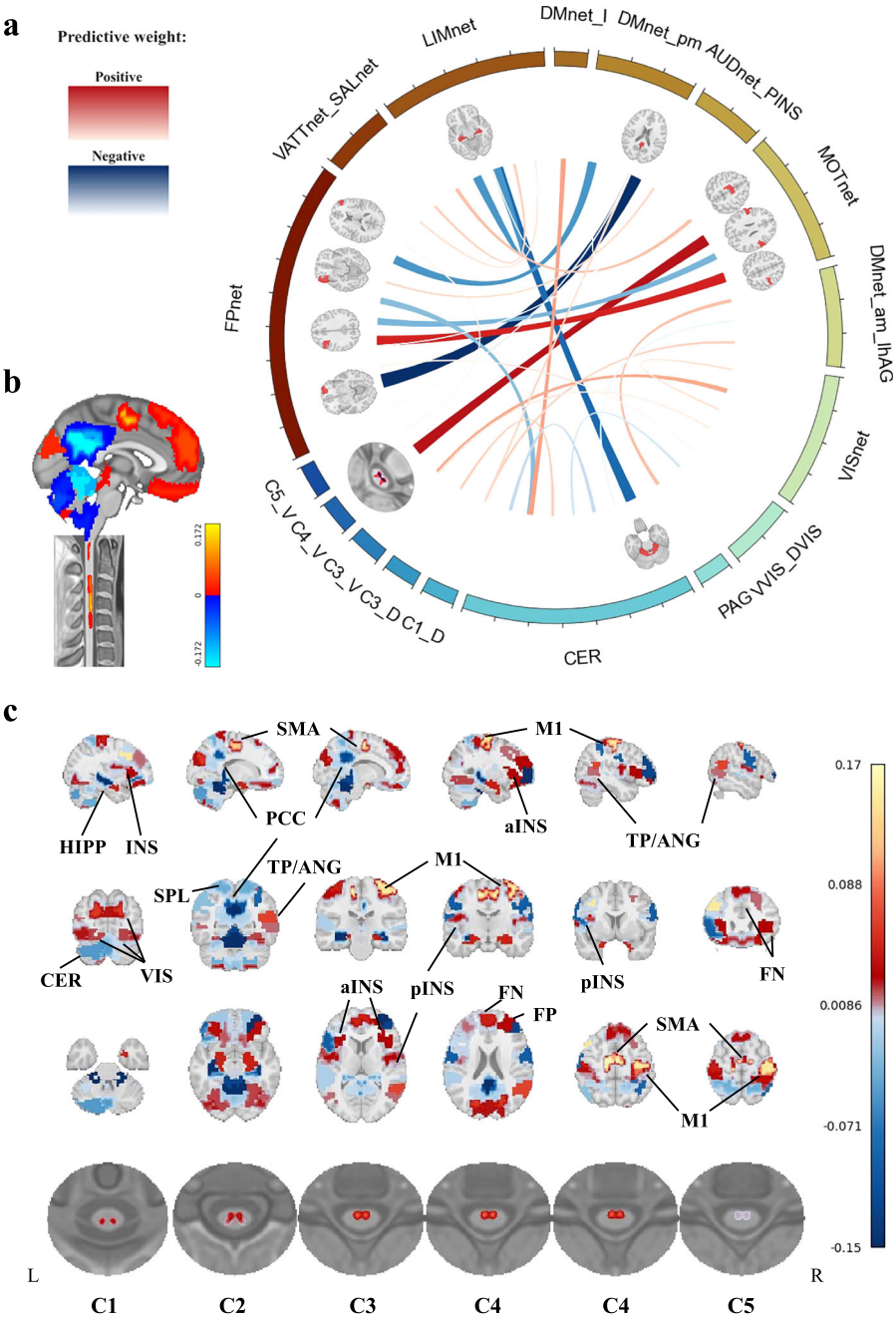

Fig. 3 | Weight structure of the CSps and parcel-level visualizations. a Chord diagram of CSps connection weights. The CSps comprises 29 non-zero corticospinal connections (16 positive, 13 negative). Edge color encodes weight sign (red = positive; blue = negative), and thickness encodes |weight |. Cortical nodes are MIST-122 parcels (displayed with macro-network color coding for orientation), together with PAG, RVM, and dorsal/ventral horns of cervical segments C1–C7; the predictive model itself is trained on 139 ROIs spanning brain, brainstem and spinal cord. Small anatomical insets depict representative high-weight links for orientation only and are not voxelwise statistical maps. **b** For interpretability, the highest-magnitude CSps connections are projected onto anatomical views of the neuraxis. **c** Parcel-level overlays of weight distribution. To complement the chord diagram, parcel-level overlays summarize the spatial distribution of positive (red) and negative (blue) weight contributions across cortex/brainstem and across cervical spinal segments C1–C5. Abbreviations. *M1* primary motor cortex; *SMA* supplementary motor area; *PCC* posterior cingulate cortex; *INS* insula; aINS/pINS, anterior/posterior insula; *HIPP* hippocampus; *TP/ANG* temporal pole/angular gyrus; *SPL* superior parietal lobule; *FP* frontal pole; *CER* cerebellum; *VIS* visual cortex; *FPnet* frontoparietal network; *SAL/VATTnet* salience/ventral attention network; *DMnet* default-mode network; *AUDnet* auditory network; *MOTnet* motor network; *LIMnet* limbic network; *PAG* periaqueductal gray; *RVM* rostroventral medulla. Source data are provided as a Source Data file.

indicate that all five models exhibited poor generalizability compared to CSps, suggesting that the performance of CSps relies on integrated connectivity between brain and spinal cord regions.

Using virtual lesion analysis[2], we identified connections critical for the CSps' predictive performance. Individually removing each of the 29 non-zero predictive weights, we found that the top five most impactful connections included those from the sensorimotor network to spinal cord C4 (Supplementary Fig. S2b). However, removing any of these did not reduce the model's performance by more than 10% of explained variance. This suggests that none of the CSps features are indispensable, highlighting the widespread distribution of pain sensitivity information across the CNS, consistent

https://doi.org/10.1038/s41467-025-67132-6

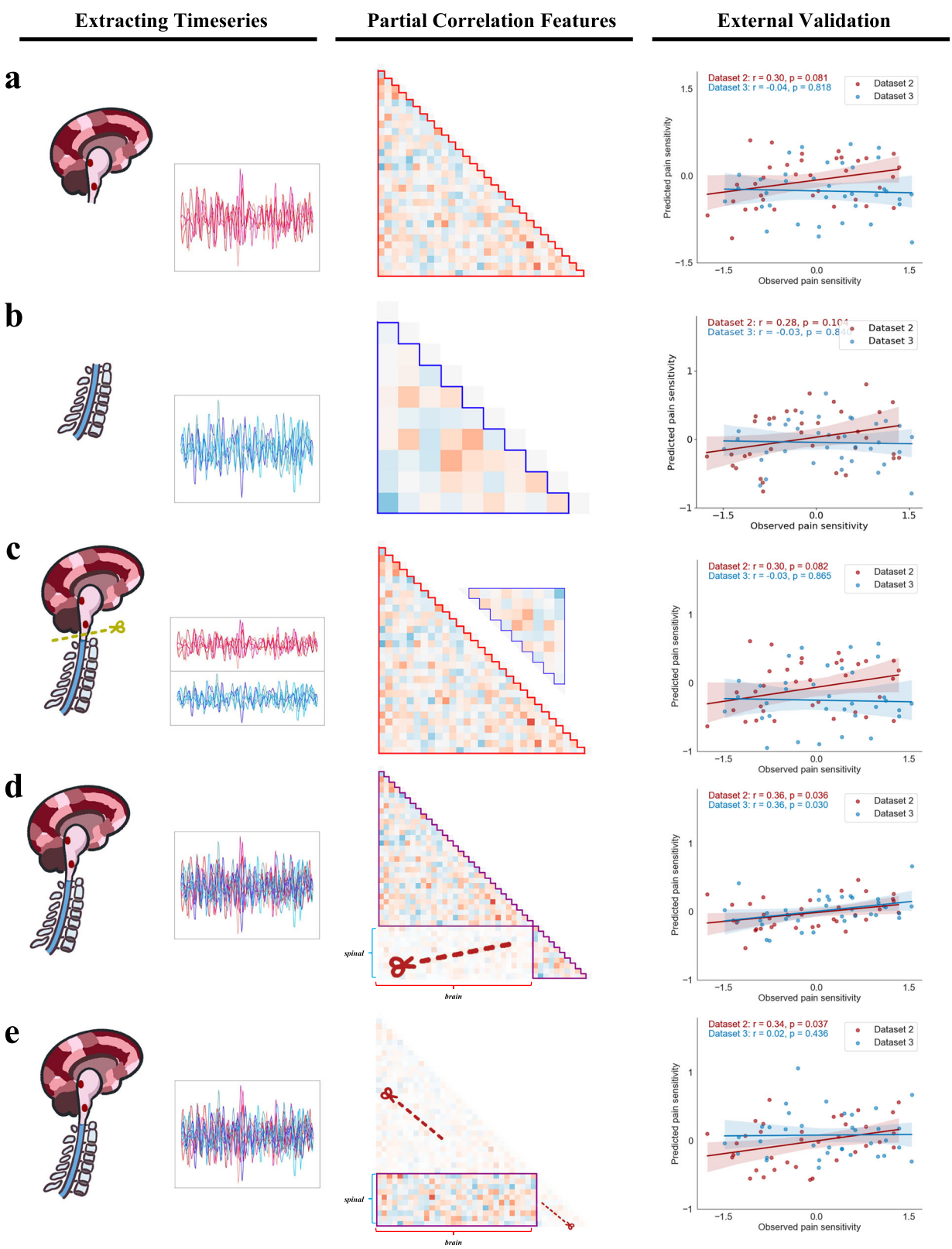

with pain pathway physiology[33–36]. We further tested the CSps' robustness by progressively removing connections until all were deleted. The explained variance decreased steadily, reaching zero after 25 out of 29 connections were removed (Supplementary Fig. S2a). Notably, when all spinal cord-related connections were removed first, the reduction in explained variance was less pronounced compared to random removal.

Clinical applicability of the CSps

After validating CSps in healthy individuals, we applied the model to a cohort of diabetic patients with chronic pain (Dataset 5, DMC, $n = 22$). The CSps successfully predicted the Short-Form McGill Pain Questionnaire (SF-MPQ) scores in DMC patients (Fig. 5a), with a Pearson correlation of 0.49 ($p = 0.009$), but did not predict non-pain-related clinical indicators (e.g., HbA1c, Glu, see Supplementary Data 5).

https://doi.org/10.1038/s41467-025-67132-6

Fig. 4 | Validation of the importance of corticospinal modeling. Panels (**a**–**e**) depict five ablation models trained on Dataset 1 and evaluated on Datasets 2–3 with the same pipeline used for the CSps. Left column: mixed ROI time series (red = brain ROIs; blue = cervical spinal ROIs). Middle column: the corresponding partial-correlation feature blocks (red = brain partial-correlation matrix; blue = spinal partial-correlation matrix; purple = corticospinal partial-correlation matrix). Because features are partial correlations, computing them with brain and spinal signals separately vs. jointly yields different estimates (the joint case mutually controls shared variance across systems); the scissor icon indicates which signals/edge classes are separated or removed prior to feature computation. Right column: external-validation scatterplots. For all external-validation scatterplots (right column), points are independent participants (Dataset 2: $n = 35$; Dataset 3: $n = 36$); regression lines depict the fitted mean with 95% CI bands. Associations are two-sided Pearson's r; *P*-values and 95% CI are reported in the panels or Supplementary Data 4. No multiple-comparison correction was applied across models (M1–M5 vs CSps) because a single primary association per dataset is presented; see Methods for the full ablation design. **a** Brain model (M1): Includes 122 regions of interest (ROIs) from the MIST atlas, the periaqueductal gray (PAG), the rostroventral medulla (RVM) and the mean gray matter of the brain, totaling 7750 features. **b** Spinal model (M2): Includes only the dorsal and ventral horns of cervical segments C1 to C7 and the average gray matter of the spinal cord, resulting in 91 features. **c** Segmented model (M3): Uses the partial correlations matrix for M1 and the partial correlations matrix for M2, giving a total of 7841 features, to eliminate the effect of the brain and spinal cord time series on each other separately. Scissor denotes the separation at the time-series level. **d** Disconnected model (M4): Similar to the original model (CSps), but excludes all connections between brain and spinal regions after computing the partial correlation matrix for 139 ROIs, eliminating 1,750 inter-regional features (14 spinal ROIs to 125 brain regions) and resulting in 7841 features. Scissor marks deletion of cross-system connections. **e** Solely-connected model (M5). Only brain–spinal edges are retained; all intra-brain and intra-spinal connections are removed. Scissor marks deletion of intra-system edges. Abbreviations. *CSps* corticospinal pain signature; *ROI* region of interest; *MIST* Multiresolution Intrinsic Segmentation Template; *PAG* periaqueductal gray; *RVM* rostroventral medulla; *MAE* mean absolute error. Source data are provided as a Source Data file.

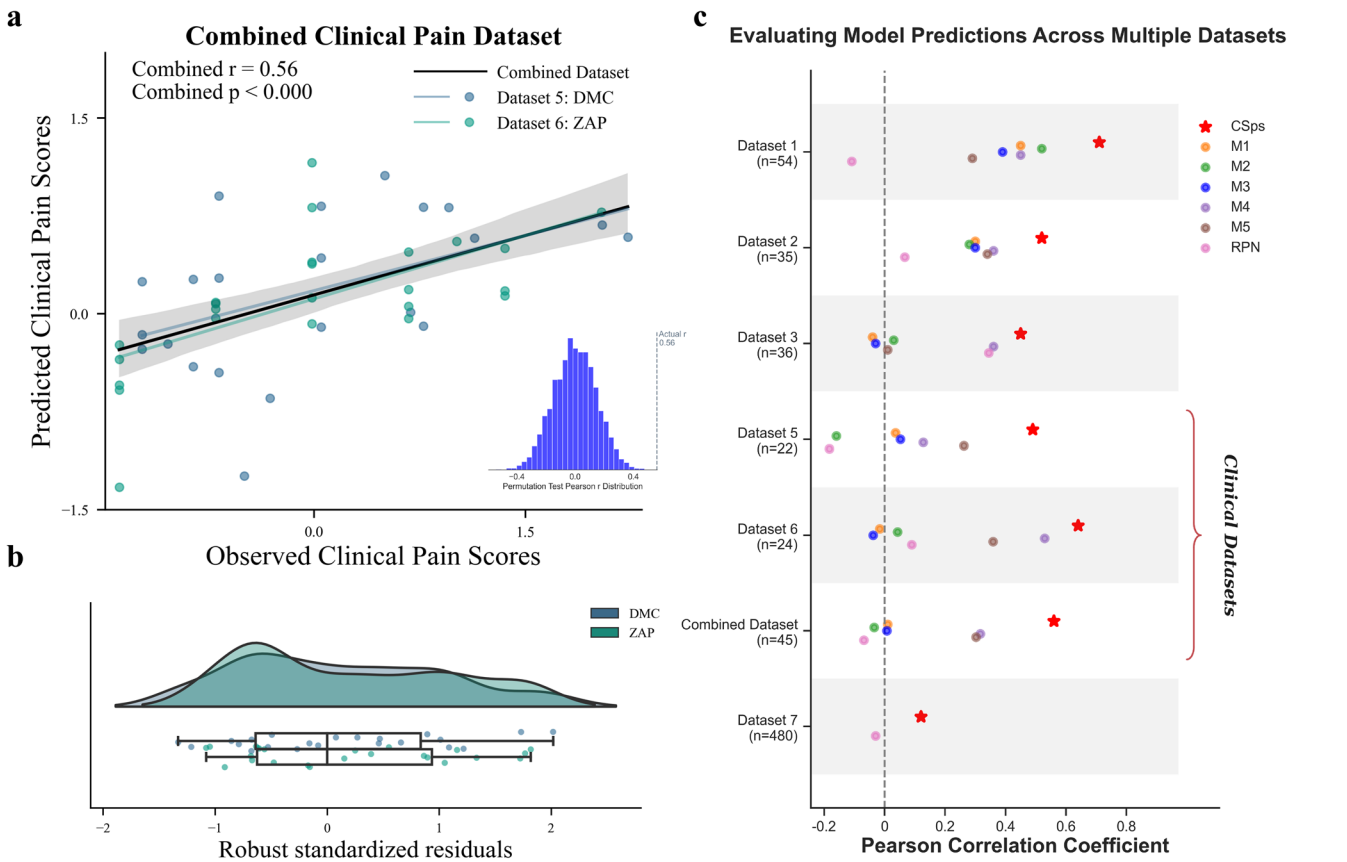

Fig. 5 | CSps predicts clinical pain and outperforms alternative models across datasets. a Combined Clinical Pain Dataset. Predictions from the corticospinal pain signature (CSps) are shown for the combined clinical dataset formed by Dataset 5 (DMC, $n = 22$; SF-MPQ) and Dataset 6 (ZAP, $n = 24$; clinician-administered NRS). Scores were within-dataset z-standardized before merging. The CSps achieved $r = 0.56$ with $p < 0.001$ and MAE = 0.73 across the combined sample (inset: permutation null). **b** Cohortwise residual distributions. Box-and-violin overlays per cohort (DMC vs ZAP) are defined as: center line = median; box = IQR; whiskers = 1.5 × IQR; points are individual patients. $n = 22$ (DMC) and $n = 24$ (ZAP); residuals are robust standardized residuals from panel a computed at the patient level. **c**, Evaluating models across datasets. Pearson's r for CSps (red stars) is contrasted with brain-only/spinal-only ablations (M1–M5) and a published RPN across multiple datasets (D1–D3, D5–D6, combined clinical, and a large brain-only dataset used for fair comparison). As reported in the text, RPN showed weak or non-significant associations in healthy and clinical datasets, whereas CSps yielded consistently higher performance; in the large brain-only dataset (Dataset 8, $n = 462$), a brain-only version of CSps (bCSps, spinal/brainstem weights removed) still outperformed RPN (bCSps: $r = 0.12$, $p = 0.006$; RPN: $r = -0.03$, $p = 0.50$). Correlations are Pearson's r with two-sided tests; exact *P*-values are provided in the figure or Supplementary Data 7. No multiple-comparison adjustment was applied across datasets; the primary inference is model-level association within each dataset. Abbreviations. *CSps* corticospinal pain signature; *bCSps* brain-only CSps; *RPN* Resting-state Pain Sensitivity Network; *SF-MPQ* Short-Form McGill Pain Questionnaire; *NRS* Numerical Rating Scale; *DMC* diabetic patients with chronic pain; *ZAP* zoster-associated pain (subacute); *MAE* mean absolute error. Source data are provided as a Source Data file.

Next, we extended our analysis to a group of patients with zoster-associated pain (Dataset 6, ZAP, $n = 24$ after exclusions). We aimed to employ the CSps model to predict NRS pain ratings in the Subacute phase. We observed that the CSps model was remarkably effective in predicting the NRS score of ZAP (Fig. 5a), with a Pearson correlation coefficient of 0.64 ($p = 0.0009$, one-sided permutation tests), illustrating the model's ability to accurately predict the NRS score.

Although DMC and ZAP may have different etiologies, previous studies have indicated that clinical pain conditions have a high degree of overlap in certain aspects[37]. For example, they share common psychosocial factors[38], genetic risk profile[39], and exhibit similar changes in the central nervous system[40,41]. We conducted within-dataset Z-score normalization of clinical pain scores (i.e., SF-MPQ and NRS-ZAP) for Dataset 5 and Dataset 6, to mitigate issues arising from diverse scoring methods. Merging these datasets, we applied CSps to predict clinical pain scores. The CSps demonstrated strong predictive performance: an MAE of 0.73, 32% variance explained, and a Pearson correlation of 0.56 ($p < 0.001$) across the combined dataset (Fig. 5a). As shown in Fig. 5b, the distribution of robust standardized residuals confirmed the model's validity, with residuals falling within a range of ± 2 standard deviations, which indicates a lack of systematic bias.

Comparisons between CSps and other models

To further assess CSps predictive performance, we compared it to the Resting-state Pain Sensitivity Network (RPN), a brain-based model for pain sensitivity[8]. RPN's predictions for thermal pain thresholds and clinical pain outcomes were poor across Datasets 1–3 ($r = -0.11$, $p = 0.43$; $r = 0.06$, $p = 0.70$; $r = 0.34$, $p = 0.04$) and clinical datasets (Dataset 5: $r = -0.18$, $p = 0.42$; Dataset 6: $r = 0.22$, $p = 0.31$; Combined: $r = -0.03$, $p = 0.81$). Models M1–M5 were also tested on Datasets 5, 6, and the combined dataset, with only M4 (disconnected model) and M5 (solely-connected model) showing marginal significance in predicting pain scores in ZAP and the combined dataset. Other models failed to achieve significance (Fig. 5c).

Directly comparing CSps and RPN is challenging because CSps encompasses more comprehensive CNS information, while most existing research datasets focus solely on brain imaging. To overcome this limitation, we utilized a large, well-established brain imaging dataset on pain (Dataset 8, $n = 462$, after exclusion), which includes cold pain threshold data and has been employed in prior studies[42,43]. For an equitable comparison, we removed weights related to the brainstem and spinal cord from the CSps, creating a brain-only version (bCSps) that aligns with RPN's features. Despite this modification, bCSps still implicitly controls for spinal cord activity due to the use of partial correlation matrices, leaving 22 significant intra-brain connectivity weights. Applying both bCSps and RPN to predict pain thresholds in Dataset 8, bCSps achieved a Pearson correlation of 0.12 ($p = 0.006$), outperforming RPN's correlation of −0.03 ($p = 0.50$). Thus, even without explicit spinal cord features, bCSps surpasses RPN, likely because it retains the advantage of controlling for spinal cord activity in its functional connectivity estimation.

Sensitivity of the CSps to rTMS-induced Pain Changes

Considering that one of the significant features of the CSps is the direct connectivity between the M1 and the spinal cord (Fig. 6a), with M1 being a key target for TMS in pain modulation[44], we collected Dataset 7 to investigate whether CSps scores are sensitive to changes in pain perception following 10 Hz rTMS stimulation. We recruited 58 participants, assigned to either an M1 group ($n = 30$) or a Sham group ($n = 28$, after exclusion). All participants underwent resting-state fMRI and an electric pain task before and after 10 Hz rTMS to assess changes in corticospinal functional connectivity and pain sensitivity, respectively (Fig. 6b).

Our results demonstrate that changes in CSps scores effectively tracked rTMS-induced alterations in pain perception, but this effect was specific to the M1 stimulation group. Specifically, the change in CSps scores was significantly correlated with the change in pain sensitivity in the M1 group ($r = 0.55$, $p = 0.002$), but not in the Sham group ($r = 0.22$, $p = 0.267$) (Fig. 6c).

To investigate the neural underpinnings of this finding, we examined changes in the M1-spinal cord functional connection (pre-rTMS minus post-rTMS), a core feature of the CSps. As visualized in Fig. 6d, most participants in the M1 group exhibited a decrease in this connection's changes compared to the Sham group. A direct between-group comparison confirmed that 10 Hz rTMS significantly reduced the changes of M1-spinal cord functional connectivity (change in Fisher's Z-transformed r-values), with a medium effect size ($t = -2.443$, $p = 0.0177$, Cohen's $d = 0.642$) (Fig. 6e). This finding is consistent with the known excitatory effects of 10 Hz rTMS on the M1 cortex[44] and indicates that the CSps is sensitive enough to capture pathway-specific functional reorganization induced by neuromodulation and its subsequent impact on pain perception.

Discussion

The CSps model integrates multilevel neuroimaging signals from the cerebral cortex, brainstem, and cervical spinal cord to estimate individual pain sensitivity. In empirical comparisons, models that incorporated corticospinal metrics showed higher predictive performance than those restricted to cerebral data when tested across independent resting-state and task-based datasets that included both healthy participants and clinical cohorts. Moreover, experimental modulation of M1–spinal connectivity with rTMS produced predictable changes in CSps scores that paralleled alterations in reported pain, suggesting a causal relationship between corticospinal coupling and pain perception. These observations identify corticospinal connectivity as a pain sensitivity biomarker that may guide neuromodulation-oriented interventions and support the broader use of combined corticospinal imaging in pain research and clinical assessment.

The utilization of corticospinal imaging over solely brain imaging addresses key limitations of prior studies that often overlooked the spinal cord's integral role in nociception and modulation[4,8,45]. By capturing the dynamic corticospinal interactions and revealing bidirectional communication, corticospinal imaging offers a more comprehensive view of pain processing, uncovering neural signatures not detectable through brain imaging alone. Our CSps model and its cortical features (i.e., bCSps) consistently outperformed models trained exclusively on non-corticospinal data across all datasets, even surpassing established models like the RPN[8] that rely solely on brain resting-state data. This superior performance underscores the potential of integrating richer neurobiological data into pain prediction frameworks and highlights the physiological significance of incorporating spinal cord information. From an information theory perspective, corticospinal connectivity features provide a higher signal-to-noise ratio by focusing on regions directly involved in pain transmission and modulation, thereby enhancing the accuracy and applicability of predictive models in both clinical settings and healthy populations[46]. Unlike the brain, which engages in complex high-level cognitive processing, the spinal cord primarily integrates and transmits sensory information, offering more direct and specific insights into pain-related neural activity. Its physiological structure is inherently oriented toward transmitting and modulating nociceptive signals, making it less sensitive to confounding effects present in whole-brain data. These considerations suggest that corticospinal fMRI data contain specific and extra information for pain prediction.

We assessed the CSps model as a potential neural marker for pain perception. Through MVPA, we validated CSps across three resting-state corticospinal datasets, confirming its robustness and generalizability. Despite the potential bias introduced by the overlap between Datasets 1 and 2[47], the unbiased Dataset 3 affirmed CSps's capacity to predict pain sensitivity, highlighting the unique role of corticospinal

https://doi.org/10.1038/s41467-025-67132-6

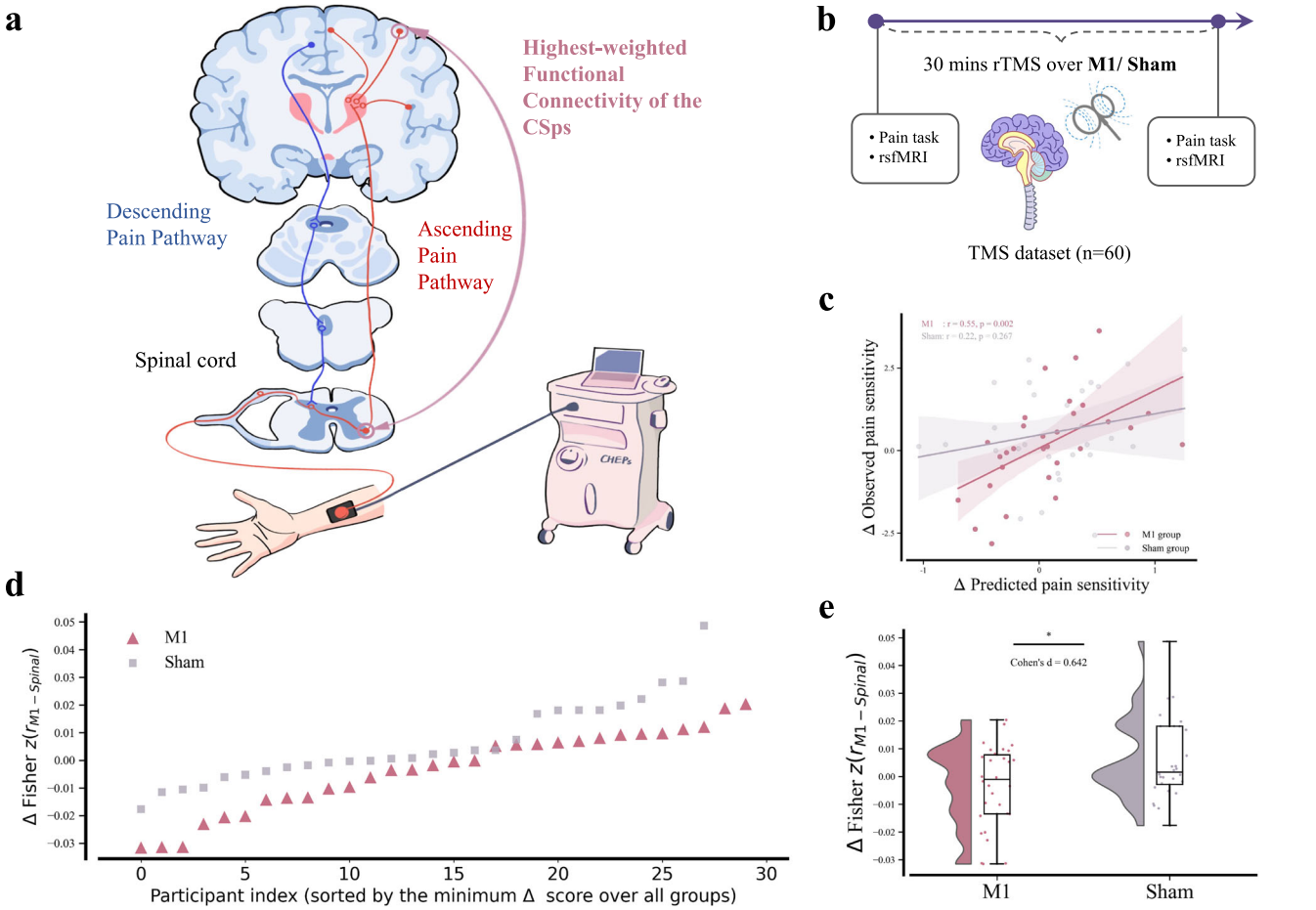

Fig. 6 | A corticospinal signature for interindividual pain sensitivity. **a** Illustrative pathways and highest-weighted CSps edge. Schematic of ascending (red) and descending (blue) pain pathways across the neuraxis. The green arc marks the highest-weighted CSps connection, linking M1 within the anteromedial somatomotor network to the C4 ventral horn (i.e., the largest-magnitude weight among the 29 non-zero CSps edges; illustration for orientation only, not a statistical map). **b** Experimental design. Participants completed a pre/post protocol with high-frequency rTMS (10 Hz) over M1 for 30 min, with resting-state corticospinal fMRI and an electrical pain task administered before and immediately after stimulation/sham. **c** Behavior–signature coupling. Scatter shows the relationship between ΔLowPain and ΔCSps across participants; solid lines depict group-wise fits (M1 vs. sham) with 95% CIs. The overall association was significant (n = 0.55, p = 0.002). We index rTMS effects with ΔLowPain (post–pre change in low-pain ratings) and ΔCSps (post–pre change in CSps score). Lines show group wise least squares fits (mean) with 95% CI bands. n = 30 (M1 rTMS) and n = 28 (sham); units are independent participants. M1 association: Pearson's r = 0.55 with p = 0.002; 95% CI for r = [0.333, 0.737]. **d**, **e** Change in the highest-weighted connection. Participant-wise change in Fisher-z connectivity is shown for M1 and sham groups (sorted in (**d**); summarized in (**e**)). These panels visualize how rTMS over M1 alters the M1–C4 ventral horn coupling emphasized by the CSps. Box-and-violin overlays summarize participant level change scores (centre line = median; box = IQR; whiskers = 1.5 × IQR; points are individuals). n = 30 (M1) and n = 28 (sham), biological replicates. Between-group comparison used an independent samples t test (two-sided) on Δ connectivity: $t(56) = -2.443$, Cohen's d = 0.642, p = 0.018, 95% CI for accuracy = [−0.017, −0.001]. CSps corticospinal pain signature, rTMS repetitive transcranial magnetic stimulation, M1 primary motor cortex, NRS numerical rating scale. Source data are provided as a Source data file.

data in enhancing pain prediction beyond conventional brain-based models. Crucially, CSps exhibited specificity to pain, as its corticospinal signature showed no significant correlation with demographic or psychological variables[8], underscoring its independence from these factors. In addition, in an independent task-based corticospinal dataset, CSps successfully discriminated between thermal pain and cold sensation tasks, further emphasizing its pain-specificity. This is significant, given that pain across different modalities often shares common neural pathways[4,34,43], yet the pain threshold is sensitive to nociceptive intensity[48]. It is important to acknowledge that human pain processing involves complex, nonlinear neural dynamics[4,9,45,49]. However, our direct comparison of the linear CSps model against nonlinear alternatives (i.e., support vector regression and random forests) demonstrated that the linear approach provided competitive, and in fact superior, out-of-sample predictive accuracy in this context. This suggests that for this high-dimensional corticospinal feature space, the primary predictive signals were sufficiently captured by a linear combination of features, with the added benefit of preserving the interpretability of individual corticospinal connections. Together, these observations indicate that corticospinal connectivity patterns capture variance related to individual pain sensitivity while remaining largely unaffected by non-nociceptive factors, a property that may support objective assessments of pain.

An important finding of our study was that intrinsic functional connectivity markers demonstrated potential for diagnosing and assessing clinical pain. Perhaps counterintuitively, features from the resting-state may predict individual differences in task-based and even clinical pain scores. However, within the field of neuroscience, there is a growing understanding of the brain as a complex, intertwined system[50,51], where perception, cognition, action, emotion, and motivation are integrated by complex brain networks. Individual differences in pain processing manifest as unique connection weights within

this elaborate network integration[2,8,52]. This may be because connections between brain networks not only transmit signals but also modulate the brain's ability to amplify or attenuate them[53]. Previous research has shown that the strength of these intrinsic network connections can predict individual differences in brain activation during tasks[7], as well as accurately predicting pain sensitivity[8], and fluid intelligence[54]. These studies inspired the construction of our model. Extending beyond prior work, we leveraged the corticospinal network. Our model successfully distinguished between pain and cold sensation conditions during tasks and predicted clinical pain scores. These findings suggest that corticospinal fMRI offers an advantage in predicting pain sensitivity and elucidating the mechanisms of pain perception, providing a more comprehensive view of pain processing by integrating both brain and spinal cord data.

The CSps demonstrated consistent predictive accuracy for clinical pain ratings across two distinct patient populations. This capability is further supported by the fact that persistent thermal pain, which is a common experimental model closely resembling clinical pain[9], validates the effectiveness of using thermal pain sensitivity data from healthy individuals to predict clinical pain. In contrast, neither the RPN model based on resting-state brain data[8] nor the non-corticospinal models we trained could successfully achieve this. Previous studies have shown that QST-derived pain sensitivity can predict clinical outcomes, such as postoperative pain[26]. Pain sensitivity is pivotal in both the onset and persistence of chronic pain, with variability among healthy individuals potentially predisposing them to chronic pain via peripheral and central sensitization[23,24]. Elevated pain sensitivity is associated with heightened acute postoperative pain and an increased risk of chronic pain development[55], as well as responses to analgesics, where efficacy reflects pain inhibition capacity, which is a key factor in chronic pain development[56]. Although our study linked QST-based sensitivity in healthy individuals to clinical pain, the absence of longitudinal data tracking pain progression from acute to chronic highlights the need for further research. Animal models support this link, demonstrating that higher thermal pain sensitivity correlates with diminished opioid efficacy and sustained pain[57]. This relationship was particularly pronounced in mice with chronic sciatic nerve injuries, who showed both heightened pain sensitivity and reduced effectiveness of morphine treatments. In contrast, mice with lower nociceptive sensitivity responded better to pain relief medications and experienced shorter durations of cancer-related pain, reinforcing the significance of pain sensitivity in chronic pain progression and treatment response.

Our findings also contribute to the broader landscape of pain prediction, which increasingly recognizes the importance of psychosocial factors. Recent work, for instance, has demonstrated that multivariate psychosocial risk scores are robust predictors for the development and persistence of chronic pain[38]. We position the CSps as a complementary, rather than competing, biomarker. Notably, CSps was not significantly associated with individual psychosocial scales in healthy individuals, suggesting it captures a distinct neurobiological variance not trivially explained by single psychological traits. While comprehensive psychosocial assessments may excel at identifying long-term risk, the CSps demonstrated specificity for predicting the severity of current clinical pain. This suggests a powerful future direction where corticospinal biomarkers like CSps are integrated with psychosocial tools to create holistic models that capture both an individual's vulnerability to chronic pain and their present clinical state.

A key finding of this study was the significant functional connectivity between M1 and the C4 ventral spinal region in the CSps, where enhanced M1-spinal connectivity correlated with increased pain sensitivity. Previous animal studies have demonstrated that indirect M1-spinal interactions influence pain modulation[55]. In humans, pain-related M1 activation has been observed through intracortical recordings and neuroimaging[58], with M1's connectivity to other brain regions predictive of pain perception[4,8]. However, no human studies have directly linked increased M1-spinal cord connectivity to pain sensitivity. Our study bridges this gap, revealing that pain-free individuals with high pain sensitivity exhibit enhanced M1-spinal connectivity, suggesting that changing this connection could reduce pain perception. This aligns with non-invasive neuromodulation studies, such as TMS, which alleviate pain by stimulating M1[44]. In addition, our results suggest that changes in the CSps scores, which reflect the connectivity between M1 and the spinal cord and other network-level connections, are correlated with alterations in pain perception induced by rTMS. This correlation further supports the notion that M1-spinal cord connectivity plays a crucial role in pain modulation, as changes in brain connectivity within this pathway were directly associated with changes in pain sensitivity. These findings provide compelling evidence that the CSps model can capture the neural changes underlying pain modulation in response to TMS, highlighting its potential as a biomarker for pain treatment efficacy. This is supported by animal models where Motor Cortex Stimulation (MCS) increased pain thresholds in rats[35], with analgesia primarily mediated through spinal neuronal activity rather than changes in neurotransmitter levels like Substance P or enkephalins. Although the precise biological mechanisms underlying M1-induced pain relief in humans remain unclear, our results underscore the role of the corticospinal pathway in pain regulation. Understanding the M1-spinal connection may thus offer insights into alternative pain management strategies that integrate motor control and pain processing.

Beyond corticospinal coupling per se, these findings should be interpreted within the canonical descending pain modulatory system (DPMS) linking cortex, PAG, RVM, and segment-resolved dorsal/ventral horns of the cervical cord[49]. Our ROI set was explicitly designed to probe this circuitry, enabling tests of how traitlike corticospinal tone interacts with descending control at the level of the cord. Prior human brainstem–cord fMRI shows that attention, value/expectation, and pharmacology can recruit PAG/RVM pathways to modulate dorsal-horn responses and analgesia[13,59]. Embedding these insights, CSps offers a systems-level readout that captures variance attributable to both descending inhibition/facilitation and direct corticospinal influences. Two observations are particularly consistent with DPMS physiology. First, the top-weighted CSps edge between M1 and the C4 ventral horn suggests that motor efferent pathways and segmental premotor circuits can bias nociceptive gain, complementing PAG/RVM-centered control rather than competing with it; noninvasive modulation of M1 has recognized analgesic effects in humans[44]. Second, rTMS over M1 produced covarying changes in CSps scores and pain ratings in our data, with concomitant enhancing in M1–cord coupling, indicating that neuromodulation can shift the net balance of descending signals captured by CSps. Together, these results support an integrated (brain + brainstem + spinal) model in which stable individual differences in DPMS efficacy and corticospinal coupling set the operating point of nociceptive inflow[49]. Brain-only or cord-only models may therefore miss inter-level interactions necessary to predict both experimental sensitivity and clinical pain. CSps operationalizes this integration in a single biomarker and provides a tractable bridge from mechanistic fMRI to neuromodulatory intervention design.

Our study has several limitations. First, the sample size, while comparable to or exceeding previous brain imaging biomarker studies, is smaller than large-scale cohorts like the UK Biobank[38]. The effect sizes might be overestimated due to the initial sample. Future research should assess the clinical utility of the CSps in larger corticospinal datasets. In addition, our sample was exclusively East Asian, potentially limiting generalizability given evidence suggesting racial differences in spinal cord injury susceptibility[60] and corticospinal pathway variability. We plan to expand testing to other populations. Next, because CSps was trained on upper-limb thermal thresholds and

relies on cervical cord measures, it may be preferentially tuned to upper-limb nociception. While the CSps significantly predicted pain severity in two independent clinical cohorts, site-specific differences in healthy cohorts require direct lower-limb validation. The lack of longitudinal data also limits our ability to track dynamic changes in corticospinal connectivity during the progression from health to chronic pain. Moreover, the predominance of young, healthy participants in our study restricts the exploration of this transition. Long-term studies are needed to elucidate the role of corticospinal pathways in chronic pain development. While our findings suggest the M1-ventral horn connection's predictive value for pain sensitivity, direct testing of its analgesic effects through methods like online TMS-fMRI[61] is necessary to validate its therapeutic potential. Finally, pain perception is a multifaceted process influenced by genetic and peripheral factors. Previous research has highlighted how genetic variations can affect pain sensitivity and analgesic efficacy[29]. Future studies should consider incorporating genetic data and assessments of peripheral nervous system function to enhance the predictive power and clinical applicability of pain sensitivity models.

In summary, corticospinal connectivity measures account for variation in individual pain sensitivity and may function as candidate biomarkers for clinical assessment. Further research should explore its application in personalized pain management and large-scale clinical settings, thereby clarifying the contribution of spinal pathways to central nociceptive processes.

Methods

Following the recent guidelines and criteria for building neuroimaging biomarkers[2,8,52], we designed this study using eight datasets, aiming to develop a corticospinal pain sensitivity signature.

Participants

For various research purposes, Datasets 1-3 were collected from the Capital Medical University of Beijing Tiantan Hospital during the period of 2019 to 2020. Dataset 1 initially included 65 participants. However, due to the absence of heat pain threshold data in 9 participants and the lack of spinal data in 2 participants, the final sample comprised 54 right-handed individuals (31 females, age = 22.25 ± 3.13). For a separate experimental objective, 35 of these 54 participants underwent a test-retest task with a two-week interval. The pre-test data of these 35 participants constituted Dataset 1, and their post-test data formed Dataset 2 (20 females, age = 22.06 ± 2.99). Dataset 3, an independent dataset, initially comprised 40 healthy participants. However, 3 individuals were excluded due to the absence of spinal cord data, and 1 individual was excluded due to the excessive head movement during scanning, resulting in a final sample size of 36 (20 females, age = 21.47 ± 3.48). Dataset 4, collected at the Biomedical Imaging Research Center at Tsinghua University, initially comprised 39 healthy participants. However, one participant was excluded due to excessive head movement, leaving 38 participants (20 females, age = 23.42 ± 2.96), who participated in both pain and cold sensation tasks.

Dataset 5 was collected from Shandong Provincial Hospital for the initial experimental purpose of exploring differences in neural mechanisms between subgroups of Type 2 diabetic patients with and without concomitant pain, unrelated to the present study, and included a total of 32 participants. All participants met the diagnostic criteria for Type 2 Diabetes Mellitus established by the American Diabetes Association in 2023[62]. Due to the specific purpose of our study, only 22 diabetic patients (9 females, age = 59.68 ± 7.95) who were still suffering from pain lasting at least three months at the time of the corticospinal scan were selected for the final analysis. Before undergoing MRI scans, clinical doctors assisted patients in filling out SF-MPQ[63]. This questionnaire measures: (1) the Pain Rating Index (PRI), comprising 15 descriptors rated from 0 (none) to 3 (severe) to reflect pain intensity over the past month; (2) a 10 cm Visual Analogue Scale (VAS) for evaluating the general present pain intensity; and (3) the Present Pain Intensity (PPI), scored from 0 (none) to 5 (unbearable) to assess immediate pain sensation. In addition, we also collected all participants' clinical indicators, such as glycated hemoglobin HbA1c (%), fasting blood glucose Glu (mg/dl), fasting total cholesterol, HDL (mg/dl), LDL (mg/dl), and triglycerides (mg/dl).

Dataset 6 specifically targets individuals diagnosed with ZAP. In this study, the ZAP classification encompassed the subacute phase (from the end of the acute phase up to three months, prior to post-herpetic neuralgia diagnosis). Neuropathic pain was evaluated by a skilled pain specialist using the NeuPSIG grading system, and pain intensity was measured via the NRS[64], obtained in the same clinical visit immediately before the resting-state scan. The inclusion criteria required participants to meet the following conditions: (1) age over 18 years; (2) diagnosis of ZAP; (3) neuropathic pain localized to the lesion area. The initial cohort included 26 participants recruited from Beijing Xuanwu hospital. Screening procedures excluded individuals with any form of neuropathy other than ZAP, those currently receiving psychotropic or analgesic treatment, patients with missing clinical data, and patients with a history of neurological, psychiatric conditions, or other pain-related medical issues in the last six months. After a thorough review of medical records and preliminary assessments, 24 patients (7 females, age = 55.79 ± 11.82) remained eligible. Neurology clinicians used a 0–10 numerical rating scale (NRS), with endpoints of 0 (no pain) and 10 (unbearable pain).

In addition to the above mentioned, the exclusion criteria for Dataset 5 and Dataset 6 were as follows: (1) a history of cerebral tumors, neurosurgical procedures, or cranial trauma; (2) presence of acute complications; (3) severe hypertension; (4) a significant history of neurological, psychiatric, or cerebrovascular disorders; (5) history of alcohol or substance abuse; and (6) with mental disorders or contraindications to MRI.

A total of 60 healthy right-handed college students were recruited at the Chongqing University Cancer Hospital for Dataset 7. The experiment was designed to investigate the effects of high-frequency rTMS on the M1. All participants were enrolled and assigned 1:1 to M1 rTMS ($n = 30$) or sham rTMS ($n = 30$). However, 2 participants from the sham group were excluded because of the poor quality of spinal cord data, resulting in 58 participants (mean age: 23.43 ± 2.62 years, 30 females). Sex distribution did not differ between groups (2 × 2 Pearson chi-squared test, $\chi^2(1) = 0.00$, $p = 1.00$, $n = 58$). Age also did not differ (two-sided independent-samples t test, $t(56) = 1.39$, $p = 0.170$). Before the main experiment, electrical pain thresholds were measured for each participant. These thresholds were used to determine the low and high pain stimulus intensities that would be applied during the experiment. Specifically, electrical stimulation was used to establish individual pain thresholds, ensuring the stimuli used during the experiment were within the participants' tolerable range. All participants were free from any history of neurological disorders, chronic pain conditions, or psychiatric illnesses, and had normal or corrected-to-normal vision.

Dataset 8 was a large dataset related to pain, collected at the Brain and Cognitive Neuroscience Research Center, Liaoning Normal University, Dalian, China, consisting of 484 participants with brain MRI scans that had been utilized in multiple studies[42,43]. In terms of behavioral data, this dataset included cold pain thresholds, which were of particular interest. We conducted a series of data cleaning procedures. Initially, we excluded 3 participants due to excessive head movement. For the cold pain threshold, we removed 7 participants with missing behavioral data and 12 outliers exceeding 3 standard deviations, resulting in 462 participants (282 females, age = 21.51 ± 4.64) with complete cold pain threshold data and MRI data (including brain T1 structural images and resting-state fMRI).

All participants in Datasets 1–8 gave written informed consent and were paid for their participation. The study was conducted in

accordance with the Declaration of Helsinki and received approval from the Ethics Committees of the Institute of Psychology, Chinese Academy of Science (Dataset 1–3: H19023; Dataset 4: H20055; Dataset 7: H24051; Dataset 8: H17025), Shandong Provincial Hospital (Dataset 5: No. 2024-398), and the Beijing Xuanwu hospital (Dataset 6: No. 2024-005-001). The study included male and female participants, with sex classification based on self-reported information. No sex-specific analyses were conducted, as the primary objective focused on identifying population-level neural signatures of pain sensitivity. No statistical method was predetermined for the sample size calculation.

Thermal pain stimulation and QST

In Datasets 1–3, thermal pain stimuli were delivered using the Pathway device (Medoc Ltd, Ramat Yishai, Israel) equipped with a 573 mm^2 (diameter 27 mm) CHEPS thermal electrode, applied to the right arm of the participants 10 cm up from their wrist. The baseline temperature was set at 32 °C, and thermal thresholds were obtained via ramped stimuli (1 °C/s), with the ramp stimulus terminated when the participant pressed a button. This procedure to assess thermal pain sensitivity was repeated a total of five times and averaged for accuracy and consistency in the measurements[65] to offer a general assessment of pain sensitivity; the within-session mean was used for analysis to reduce random error. Prior work indicates that thermal pain thresholds can achieve moderate-to-good test-retest reliability when procedures are standardized[66–68].

In Dataset 8, the Cold Pressor Test (CPT) was employed to assess participants' pain thresholds. Prior to the commencement of the experiment, participants were instructed to immerse their left hand in water maintained at 22 °C for 30 s. This was done in order to standardize the initial hand temperature[43]. Subsequently, participants submerged their left hand into cold water maintained at 2 ± 0.1 °C, instructed to immerse it to a depth of at least 3 cm above the wrist. This was done using a circulating water bath system (DX-208 water bath, Beijing Changliu Scientific Instruments Co., China), with a water flow rate set at 15 L/min. Throughout the process, participants were required to focus on the sensation in their hand and to report when they first felt pain. To ensure data precision, an experimenter stood a few feet behind the participant and used a stopwatch to accurately record the time. The pain threshold was calculated as the duration from the moment the left hand was immersed in the water until the participant first experienced pain. To ensure participant safety, if a participant did not terminate the test voluntarily within 300 s, the test would automatically terminate at the 300-second mark[43].

We applied Z-score normalization to the pain thresholds in Dataset 1. Subsequently, we standardized the pain thresholds in Datasets 2 and 3 using the mean and standard deviation from Dataset 1. To align the directionality of changes in pain sensitivity with changes in functional connectivity (i.e., stronger functional connectivity predicting higher pain sensitivity), we multiplied the sensitivity scores by negative one (i.e., $zscore(pain\ threshold) * -1$). This adjustment was purely mathematical and did not affect subsequent model development, validation, or the estimation of predictive features. Throughout, pain sensitivity refers to nociceptive sensitivity indexed by the heat-pain threshold measured with the method of limits in healthy participants.

Experimental design

Dataset 4 included two tasks: a heat pain task and a cold sensation task. These tasks were presented in a pseudo-random order to balance the sequence among participants, with rest periods between each scan interval. The heat pain stimulus was delivered using the Pathway system (Medoc Ltd, Ramat Yishai, Israel) with a CHEPS thermode (573 mm^2, diameter 27 mm), targeting the C5-C6 dermatome on the participants' right forearms. While lying on the scanning bed, participants received a series of random intensity heat pain stimuli. Starting from a baseline temperature of 32 °C, the heat stimulus increased rapidly at 40 °C/second to the target temperature, held for 10 seconds, and then returned to baseline at the same rate. We selected stimuli rated by participants at least three times as 3 (low pain) and 5 (high pain) on a numerical rating scale (NRS). The formal experiment included 30 stimuli presented in a pseudo-random order: 15 low pain and 15 high pain stimuli. Each trial began with a 6-second fixation point, followed by a 10 s pain stimulus. Participants then rated the pain intensity within 4 seconds using a button box and the NRS, which was defined as follows: 0 (no pain), 1 (just noticeable pain), and 10 (unbearable pain). For the cold sensation task, the stimulus also started at a baseline of 32 °C, rapidly decreasing at 40 °C/second to the 25 °C temperature. Unlike the heat pain task, the cold sensation was maintained for 20 s to match the baseline duration.

Dataset 7 utilized a pre-post study design to investigate the impact of rTMS on spontaneous neural activity in response to a pain task. Two fMRI scans were performed: one before the application of rTMS and one immediately after. The main objective was to assess the changes in brain activity during resting-state fMRI following rTMS-induced brain stimulation, focusing on how these changes relate to pain perception. The session comprised: (i) pre-stimulation electrical-pain task → pre-stimulation corticospinal rs-fMRI; (ii) real or sham rTMS over left M1; and (iii) post-stimulation electrical-pain task → post-stimulation rs-fMRI. Electrical stimulation was delivered using a square wave, with a frequency of 100 Hz and a pulse width of 2000 μs. The stimulation was applied in an anodal direction, and a total of 500 pulses were administered during each session. These parameters were chosen to ensure a consistent and controlled application of electrical stimuli, designed to elicit reliable responses for the study's objectives. Participants rated their pain experiences using a numerical rating scale (0–10), where 0 represented no sensation, 1 indicated mild tactile sensation, 2 corresponded to moderate tactile sensation, 3 to a noticeable touch, 4 marked the onset of pain, and 10 represented intolerable pain. Ratings between 4 and 10 indicated varying degrees of pain intensity. In this task, participants were required to rate the subjective intensity of electrical stimulation applied to their right forearm (10 cm above the wrist). The pain intensity was set to two levels: low pain (5 out of 10) and high pain (8 out of 10), with an inter-stimulus interval of 5 seconds. The final electric intensity of each participant for each level (low and high) was measured before the task as the average of at least three identical pain intensity ratings. Prior to the main experimental session, participants completed a practice run consisting of four trials. This session mimicked the experimental procedure but with fewer trials, allowing participants to familiarize themselves with the task. The formal pain task consisted of 30 trials, with a pseudo-randomized sequence of low and high pain intensity stimuli. Each trial involved the presentation of pain stimuli, after which participants rated their perceived pain intensity using the same 0–10 scale. Following the pain stimulus, participants rated their pain intensity 5 s later, according to the threshold set during the training session. Stimulus presentation and behavioral data collection were controlled using E-Prime 2.0 (Psychology Software Tools). After the task, resting-state fMRI scans were conducted. During the resting-state scans, participants were instructed to remain still with their eyes closed and avoid thinking about any specific task. This allowed for the assessment of spontaneous neural activity during baseline and post-stimulation conditions.

TMS/sham protocol

The TMS was administered using the Magstim Super Rapid2 stimulator (Magstim Company Ltd., UK), paired with a 70 mm 8-shaped coil. The coil was tracked and recorded via the Visor 2 frameless computer-assisted stereotactic neuronavigation system (ANT Neuro, Netherlands). High-frequency rTMS (10 Hz) was applied to the M1 cortex at 90% of the resting motor threshold (RMT) for 5 s, with a 25 s

interstimulus interval, over 60 sequences. RMT was determined based on the method outlined by the International Federation of Clinical Neurophysiology (IFCN) using the visible motor threshold of the left hand. High-resolution T1-weighted structural images of the subject were imported into Visor2, with M1 localization performed by an imaging specialist from the Chongqing University Cancer Hospital. RMT was determined through a stepwise increase in stimulus intensity until visible finger twitching occurred in at least 5 out of 10 trials, at which point the intensity was considered the subject's RMT. Subsequently, 30 min high-frequency rTMS was applied at 90% RMT to the M1 cortex. Following rTMS, subjects immediately underwent post-stimulation fMRI scans.

Sham stimulation was delivered with the manufacturer-matched dedicated sham coil, which is identical in appearance and placement to the active 70 mm 8-shaped coil but does not deliver an effective magnetic field to the cortex. The sham coil reproduces the acoustic click and operating sounds of active rTMS to preserve auditory cues while preventing magnetic induction in neural tissue. For each participant, the sham coil was positioned over the same left M1 target and with the same handle orientation as in the active condition; stimulation timing and train structure (number of trains, inter-train interval, and nominal device output) were programmed to match the active protocol so that only the presence of the effective magnetic field differed between groups. Participants and outcome assessors were blinded to group assignment; the coil operator was necessarily unblinded for safety and device setup.

MRI data acquisition

All corticospinal datasets (i.e., Datasets 1–7) were acquired using 3 T Siemens Prisma MRI scanners, equipped with a standard 64-channel head and neck coil. Participants were placed in the scanner and were instructed not to move their heads and not to gag during the scanning process. Foam pads were placed under and beside their heads to elevate and stabilize the cervical spine and reduce image distortion and physiological noise. A neck brace limited head and neck movement, and foam earplugs protected the participant's hearing.

High-resolution corticospinal T1-weighted anatomical images ($1 \times 1 \times 1\,mm^3$) were acquired using a 3D MPRAGE sequence with parameters included sagittal slice orientation, TR: 2300 ms, TE: 2.28 ms, TI: 900 ms, FOV: $192 \times 288 \times 288\,mm^3$, FOV phase: 100%, and flip angle: 8° (Supplementary Fig. S3a).

We utilized a modified corticospinal resting-state and task-based fMRI protocol based on the Siemens SMS-EPI sequence to simultaneously capture the brain and cervical cord's BOLD response (Supplementary Fig. S3b). The field of view (FOV) was expanded to $192 \times 192\,mm^2$, covering the entire brain and cervical spinal cord (C1-C7) with 70 slices, each 4 mm thick. A 3D shimming volume focused on the brainstem and cervical cord, with the phase coding direction set from posterior to anterior (P → A), flip angle at 80°, FOV phase at 100%, and in-plane resolution at $1.5 \times 1.5\,mm^2$. To enhance efficiency, a simultaneous multiband GRAPPA parallel imaging technique with an interleaved multi-slice mode and an acceleration factor of 2 was applied, achieving a repetition time (TR) of 2680 ms and an echo time (TE) of 27 ms. In total, 200 volumes were scanned for Dataset 1 ~ 3, 5, and 235 volumes were scanned for Dataset 4, 6. During the resting-state fMRI scanning, participants were instructed to relax and remain still with their eyes open, not to fall asleep, and not to think about anything.

To correct distortion around the brain and cervical spine caused by the extended FOV and magnetic field inhomogeneities, two opposing phase encoding B0 images were employed (for details, see data preprocessing; for correction effect, see Supplementary Fig. S3c). These images, with TR: 7500 ms and TE: 87 ms, used a 2D SP-EPI sequence, maintaining the protocol's FOV, resolution, echo spacing, acceleration, and shimming.

Physiological data, including respiratory and cardiac rates, were monitored at 400 Hz using a pulse oximeter and respiratory belt under the Siemens Physiological Monitoring Unit (PMU). Physio log files generated physiological noise regressors during fMRI data processing.

Brain MRI data (Dataset 8) were collected using a 3.0-Tesla MRI system (Discovery MR 750; General Electric Healthcare, Milwaukee, WI, USA) with an 8-channel head coil and the restraining foam pads to minimize head motion and scanner noise. High-resolution T1-weighted structural brain images were acquired using a gradient echo (3D SPGR) sequence with the parameters included sagittal slice orientation, TR: 2000 ms, TE: 2 ms, TI: 450 ms, FOV: $176 \times 256 \times 256\,mm^3$, FOV phase: 100%, and flip angle: 8°. Resting-state functional images were collected over ten minutes using an echo-planar imaging sequence with parameters included TR: 2000 ms, TE: 29 ms, flip angle: 90°, field of view: $192 \times 192\,mm^2$, in-plane resolution: $3 \times 3\,mm^2$, slice thickness: 3 mm.

MRI data preprocessing

Each sequence's raw MRI images of the brain and spinal cord were stored in individual DICOM files and converted into NIFTI format using dcm2niix (version 1.0.20230411). All corticospinal data were preprocessed using a combination of tools: deepbet[69], Spinal Cord Toolbox (SCT; version 6.1), FMRIB Software Library (FSL; version 6.0.5), and custom scripts written in Python (version 3.9.12). To ensure the accuracy of the preprocessing results, quality control was systematically implemented after each step. The detailed process is as follows:

For each participant's corticospinal structural MRI image, the process began by visually recording the upper z-axis coordinate of C1 and then segmenting the image into the brain and the spinal cord. For the brain's 3D structural data, skull-stripping was performed using deepbet, followed by the segmentation of white matter, gray matter, and cerebrospinal fluid using FSL FAST. In the case of the spinal cord 3D structural data, segmentation was carried out using SCT to obtain a binary mask of the spinal cord. Then, the result was visually inspected and manually corrected as necessary, based on segmentation quality. Subsequently, intervertebral discs were visually marked to straighten the spinal cord. Individual space structural images were then aligned to the standard vertebral stages using affine transformations, followed by a non-rigid transformation to register the images to the spinal cord standard template (PAM50 T1-weighted template).

For each participant's corticospinal fMRI images, we initially preprocessed the collected respiratory and cardiac signals using custom Python scripts. Specifically, we aligned the time of scanning and respiratory and heartbeat signals to create a trigger acquisition signal file, and modeled them using FSL PNM (Physiological Noise Modeling). PNM assumes the physiological processes to be quasi-periodic, allowing modeling based on the phase of respiratory and cardiac data through low-order Fourier series[18]. In addition, high-order Fourier terms and interactions between respiratory and cardiac cycles were included, amounting to 32 noise regressors. Global physiological noise was removed from the corticospinal fMRI images using custom Python scripts, followed by image reconstruction into NIFTI format using the Python Nibabel library (https://github.com/nipy/nibabel).

Subsequently, distortion correction in the X and Y dimensions of the fMRI images was conducted using two opposing-phase-encoding corticospinal B0 field images, employing FSL topup. Next, FSL melodic was used to decompose individual 4D corticospinal fMRI images into different spatial and temporal components, manually excluding remaining noise. The denoised fMRI images underwent slice time correction using FSL and despiking using AFNI. Finally, after visually recording the upper z-axis coordinate of C1 in the fMRI images, they were segmented into the brain and spinal cord for subsequent preprocessing.

For the brain's resting-state fMRI images, head movement was first corrected using FSL MCFLIRT. To mitigate the artifacts and noise induced by head motion more effectively, we utilized the FSL-AROMA

tool for data denoising. Subsequently, the nuisance masks for CSF and WM were registered back to the individual functional space. Time series were extracted using FSL's fslmeants, and regressed out using FSL's fsl_regfilt. The images were further smoothed with a 5 mm full-width at half-maximum (FWHM) Gaussian kernel to enhance the signal-to-noise ratio. Then, a high-pass filter with a cut-off period of 100 s was then applied to the fMRI data to remove low-frequency signals, thereby reducing the impact of non-neuronal noise and improving the temporal stability of the data. Finally, individual functional space data were aligned to individual structural spaces using ANTsPy, followed by rigid, affine, and non-linear registration to the standard MNI (2 mm) brain template. For the task-based brain data (Dataset 4), we did not perform AFNI despiking, FSL-AROMA, or the removal of the WM signal.

For the spinal cord's resting-state fMRI images, motion correction was initially performed using SCT, calculating a cylindrical mask automatically drawn along the spinal cord's central axis to exclude areas outside the spine. Spatial smoothing was then applied along the x and y-axis, using a 2D Gaussian kernel with an FWHM of 3 mm. To account for noise presented in the CSF, an additional regressor was computed using the CSF signal (top 10% variance in the average time series of CSF voxels), and the x and y translation generated by motion correction at each time point were regressed in the signal. Subsequently, the time-averaged images, post-motion correction, were manually segmented for the spinal cord using custom Python scripts. Finally, two-step registration of the spinal cord fMRI was conducted using SCT: individual structural space to PAM50 standard space and individual functional space to individual structural space. For the task-based spinal data (Dataset 4), we did not regress out the x and y translation.

MRI Image quality metrics

Supplementary Fig. S3c illustrates the impact of distortion correction on brain and spinal cord images. The first column shows T1-weighted images with segmented brain and spinal cord regions (red). The original EPI images (second column) exhibit noticeable posterior spinal cord distortion. The B0-corrected EPI images (fourth column) effectively align functional images with structural references, significantly reducing distortions in both the frontal brain regions and spinal cord.

Specifically, using Dataset 1, we first applied FLIRT to linearly register the T1-weighted brain and spinal cord structural images to the EPI space, providing reference images for comparison with functional data. Two sets of functional images, original and B0-corrected, were compared to T1 structural masks in EPI space. For both brain and spinal cord regions, we calculated the Dice similarity coefficient (DSC), which quantifies the overlap between each functional image and its corresponding structural mask. The intersection of the functional images and the structural mask was calculated, and the volume of overlapping voxels within each mask was determined. Each participant's original, B0-corrected, and field map-corrected functional images were transformed into masks and compared with the spinal cord T1 mask in EPI space. Results indicated significant differences between the original and B0-corrected images in both brain and spinal cord regions (Supplementary Fig. 3d, e).

Regions of interest definition

Machine learning analyses using neuroimaging data are vulnerable to the curse of dimensionality. Voxel-level imaging data contain hundreds of thousands of features. Brain segmentation reduces dimensionality by partitioning the brain into tens or hundreds of regions or networks[9,70]. In this study, the brain was segmented into 122 regions of interest (ROIs) based on the Multiresolution Intrinsic Segmentation Template (MIST) brain atlas[70] (Supplementary Data 6). The MIST atlas was specifically chosen as its parcels are defined by functional homogeneity, ensuring the validity of connectivity analyses. Furthermore, to investigate the core components of the pain descending inhibition system, we specifically included the ventrolateral PAG and the dorsal marginal zone of the RVM in the brainstem[33,71]. The mask for PAG was obtained from previous studies[71], while the RVM was masked using hand-drawn anatomical masks, referenced from Duvernoy's Brainstem Atlas. All 124 ROIs were transformed into individual functional spaces, serving as individualized masks to extract the time series of each ROI.

In this study, we segmented the C1 to C7 segments of the spinal cord into 14 areas, including the ventral and dorsal horns of each segment. These masks were based on a probabilistic gray matter atlas, integrated with the MNI-Poly-AMU spinal cord template[72]. The template was registered from the standard template space to each participant's individual functional space. Within this individual space, the gray matter with the highest probability in each z-slice was selected to ensure the presence of at least one voxel in each of the four gray matter horns per slice. Through slice-by-slice inspection, minimal manual editing was performed to eliminate overlaps between adjacent segments and to ensure a minimum one-voxel gap between the horn-to-horn distance (i.e., dorsal-dorsal, ventral-ventral, within-hemicord dorsal-ventral). Subsequently, the individualized masks for the dorsal and ventral horns were combined, respectively. The time series for each ROI, averaging the signals within the voxels of both the dorsal and ventral horns, were then extracted for each C1 to C7 segment.

Furthermore, in defining the ROIs, we considered the global gray matter signal as a confounding factor, while also treating it as a focal point of study due to its potential representation of processes related to alertness[73]. Under this methodological framework, each individual had a total of 139 ROIs.

Functional connectivity analysis

In this study, we constructed corticospinal resting-state functional connectivity matrices for each participant using partial correlation. Specifically, the computation of functional connectivity employed the partial correlation method, implemented through Python's nilearn package (https://github.com/nilearn/nilearn). This approach aimed to more accurately estimate the direct connection strength between node time series. Compared to full correlation, partial correlation can better capture the functional significance between nodes and is also expected to eliminate any residual global signal fluctuations shared among ROIs, such as residual motion or physiological noise effects[74]. Finally, we used static, time-averaged functional connectivity to align our methodology with the predictive target: a stable, enduring trait.

To better capture changes in task-based dynamic functional connectivity, we applied the DCC analysis method from Lee et al. [9] to Dataset 4. DCC is based on the generalized autoregressive conditional heteroscedastic (GARCH) and exponentially weighted moving average (EWMA) models (https://github.com/canlab/Lindquist_Dynamic_Correlation). In this study, we also assumed that the EWMA model parameters remain consistent across all connections. Compared to traditional sliding window functional connectivity, DCC offered better sensitivity, specificity, and test-retest reliability in detecting dynamic changes in non-stationary data correlations[9].

All processes generated a 139×139 connectivity matrix for each participant, from which we extracted and vectorized the lower triangular matrix, yielding 9591 functional connectivity features.

Developing a corticospinal resting-state signature for pain sensitivity

We used the lower triangular matrix of the partial correlation functional connectivity matrices from 54 participants (after exclusions) as feature values for predictive modeling in machine learning, aiming to predict individual heat pain threshold. Using Python's scikit-learn library (version 1.3.0, https://github.com/scikit-learn/scikit-learn), we constructed a machine learning pipeline as in a previous study[8]. Specifically, the pipeline included robust feature scaling (i.e., removing the median and scaling the data according to the quantile range), K best

feature selection (i.e., selecting the number of top features based on their importance or relevance to the pain threshold), and application of the Elastic Net regression model—a linear model combining L1 and L2 regularization. The choice of Elastic Net regression model was based on previous studies[8], primarily for its ability to adjust sparsity (i.e., the L1 and L2 regularization) as a hyperparameter, avoiding any a priori assumptions about the underlying data sparsity. As a result, this model has the ability to handle high-dimensional and potentially collinear data while maintaining coefficient-level interpretability, which is crucial for neurobiological insight. To confirm that this linear approach did not sacrifice predictive power, we empirically compared its performance against standard nonlinear models, which confirmed its competitive accuracy in our high-dimensional feature space (see Results section for full comparison). Mathematically, the objective of Elastic Net regression is to minimize the following function:

$$Loss = \frac{||y - Xw||_2^2}{2n} + \alpha^*l1\_ratio^*||w||_1 + 0.5^*\alpha^*(1 - l1\_ratio)^*||w||_2^2$$

where n is the number of samples; y is the vector of true values; X is the feature matrix containing feature values for each sample; w is the model's weight vector; and Xw represents the predicted values calculated using the model weights.

The free hyperparameters in the machine learning pipeline included the number of pre-selected features (K), the L1/L2 regularization ratio (l1_ratio), and the regularization weight (α). These were optimized using Grid Search and mean absolute error (MAE)[8] as the cost function. The range for K was set at [10, 20, 30, 40, 50, 100, 150, 200, 1000, 2000, 3000, 4000, 5000, 7000, 7500, 8000, 9000], for l1_ratio at [0.0001, 0.1, 0.25, 0.5, 0.75, 0.999], and for α at [0.001, 0.005, 0.01, 0.05, 0.1, 0.5, 1, 5]. Hyperparameter optimization was achieved through leave-one-out cross-validation, where in each internal validation loop, one participant was held out as validation data and the rest as training data. This cross-validation integrated the complete machine learning process to avoid dependencies between training and test samples. Ultimately, grid search results identified the optimal hyperparameter combination as $K = 2000$, l1_ratio = 0.999, and $\alpha = 0.1$.

To assess whether our model's predictive capability exceeds random chance and to ensure an unbiased cross-validation, we employed a one-sided permutation test for model significance. This choice is grounded in our null hypothesis, which is the model have no capacity to predict true thermal threshold, leading to no difference between the MAE of the true value and the original predicted value and the MAE of the permuted true value and the predicted value. We conducted the permutation test by shuffling the participant labels of actual and predicted heat pain thresholds over 10000 iterations.

To evaluate the stability of the predicted non-zero weighted functional connections, we conducted a bootstrapping with conditional coverage. This process involved generating 10,000 resampled samples (see Supplementary Data 3 for bootstrapping results), each equal in size to the original dataset, by randomly selecting and replacing observations with replacements from the original dataset. We then fitted the predictive model, employing the optimal hyperparameters, to each sample. Subsequently, we calculated uncorrected p-values for each selected functional connection, based on the proportion of weights that were either above or below zero[4]. However, due to the constraints of the feature selection process, the p-values and confidence intervals of the permutation tests are limited[8]. Finally, we named this predictive model the Corticospinal Pain Sensitivity Signature (CSps), with all references in the paper adhering to fixed optimal parameters ($K = 2000$, l1_ratio = 0.999, and $\alpha = 0.1$) as determined by the leave-one-out cross-validation grid search optimization. We visualized the predictive interregional connections from the CSps as a ribbon plot using the custom code (Fig. 3a). To illustrate the spatial distribution of this predictive power, we also generated a regional predictive strength map. First, we transformed individual brain region masks into a standard space probability map, which accounted for co-registration accuracy and individual anatomical variability. This probability map was then weighted by the sum of the corresponding regression coefficients (Fig. 3bc). In addition, network-level visualization followed the Yeo-7 large-scale cortical template: each atlas ROI was assigned to the network with which it exhibited maximum voxel-wise overlap, and ribbons/parcels were colored and grouped accordingly[75]. This network label was used for display only and did not affect model estimation, which operated on the original ROI set.

To evaluate CSps' generalizability in new data, we initially validated the post-test data from participants in the training set who participated in the retest experiment (Dataset 1). Specifically, we conducted external validation with post-test data from 35 participants (Dataset 2), applying feature scaling and selection from the training set to Dataset 2. This involved calculating the dot products between each functional connectivity vector and the non-zero feature weights calculated from the training model. We compared predicted and original thermal pain thresholds using MAE. Subsequently, a permutation test was performed, involving 10000 random shuffles of the 35 participants' thermal pain threshold data, predicting outcomes for these resampled datasets, and calculating post-permutation MAEs.

Despite no direct data leakage from the external validation Dataset 2 to the model-fitting procedure during training, the participants' pre-test data contributed to the development of the training model. Given that pre- and post-test data for the same participant in a test-retest experiment may exhibit similar features[47], Dataset 2 might not conclusively demonstrate CSps' effective generalizability. For an unbiased evaluation of CSps' predictive performance, we collected data from 40 healthy college students at Beijing Tiantan Hospital, Capital Medical University, in 2019. Excluding 3 participants for incomplete spinal cord imaging and 1 participant for excessive head movement, we tested CSps on the remaining 36, whose data were new to the model's training and internal validation. Dataset 3, therefore, offers a robust foundation for assessing model generalizability, along with unbiased estimates of sensitivity and specificity. Then, we applied the training set's feature scaling and selection to Dataset 3, computed dot products between each functional connectivity vector and the non-zero feature weights, and employed a permutation test with 10000 shuffles to determine the significance of the predicted original MAE.

Corticospinal functional connectivity importance analysis

To test the sensitivity and specificity of CSps regarding the dependence on connectivity between the brain, spinal cord, or both, we conducted four models using the data from the training set (Dataset 1, $n = 54$).

Model M1, named the 'Brain Model,' includes only 122 ROIs from MIST atlas, PAG, RVM, and the average brain gray matter, resulting in 7750 features; Model M2, named the 'Spinal Cord Model,' includes only dorsal and ventral horns of the C1 to C7 segments in the cervical spine, resulting in 91 features; Model M3, named the 'Segmented Model,' is built on partial correlations calculated for 125 areas of the brain (including MIST−122, PAG, RVM, and the entire brain gray matter), and then combing these with the partial correlations calculated separately for 14 areas of the spinal, totaling 7841features (i.e., features of M1 add features of M2); Model M4, named the 'Disconnected Model,' is similar to the original model but removes all connections between the brain and spinal cord after calculating the partial correlation matrix for the 139 regions of interest, specifically removing 1750 (14×125) feature values from both upper and lower triangular matrices, resulting in 7841 features; M5 (Solely-connected Model): Similar to the M4, but additionally removes all intra-brain and intra-spinal connections, creating a model where there are no internal connections within the brain or spinal cord.

Lastly, we followed the training and external validation process of CSps for these four models, including grid search for hyperparameter optimization and all tests mentioned before, such as permutation testing and external validation on Datasets 2 and 3. Note that for M1, M2, M3 the maximum value for K for feature selection in grid search is 7500, and for M2 the range of K in grid search is 5-100.

Finally, considering the varying sizes of each dataset, we used weighted explained variance to represent the overall generalization performance of each model:

$$E_w = \frac{Expl.Var._2 * N_2 + Expl.Var._3 * N_3}{N_2 + N_3}$$

Clinical applications of CSps

To assess the clinical utility of CSps, we evaluated the SF-MPQ scores (summation of the sensory, affective subscale and visual analogue scale) in Dataset 5 ($n = 22$) as these measures represent the extent of chronic pain[63]. In addition, predictions were extended to non-pain clinical markers in diabetics. Further analysis involved Dataset 6 ($n = 24$), focusing on NRS scores. Finally, we merged SF-MPQ scores from Dataset 5 with NRS scores from Dataset 6 into a merged dataset ($n = 46$), standardizing values via with-in-dataset z-score normalization. Following established protocols, we applied feature scaling and selection from the training set to the prediction samples, calculated the dot product between the non-zero feature weights and the functional connectivity vector, and computed the MAE and Pearson correlation between the real and predicted values. Lastly, we employed a permutation test with 10000 shuffles to determine the significance of the original MAE.

Model competition

Finally, to fairly compare the predictive performance of CSps with other brain models like RPN[8], we used RPN and a revised version of CSps that included only the brain-related weights, excluding those related to the spinal cord, PAG, and RVM, resulting in 22 non-zero weights, which we named bCSps. We then tested the predictive performance of bCSps and RPN on Dataset 8 for cold pain thresholds. In addition, we evaluated RPN's predictive performance on Datasets 1-3. Lastly, we tested M1-5 and RPN on clinical datasets. Pearson correlation was used to assess the linear relationship between the predicted and actual values of the two models.

Statistical analysis

All data preprocessing and statistical analyses were conducted using Python (version 3.9.18) and its libraries, including NumPy, SciPy (version 1.13.1), antspyx (version 0.4.2), nibabel (version 5.2.1), nilearn (version 0.10.3), and scikit-learn (version 1.3.0). Pearson correlation was used for assessing the relationships between continuous variables, while logistic regression was applied to examine the associations with binary variables, with significance assessed via a 10000 times permutation test using SciPy's permutation_test function. Task-based data were evaluated using the binomtest function in SciPy. Partial correlations within functional connectivity data were calculated using Nilearn's Connectivity Measure function. Model significance was tested with 10000 times permutation tests on both r-values and MAE. Although no sex-specific analyses were conducted, as the primary objective focused on identifying population-level neural signatures of pain sensitivity, the aggregated sample accross the main datasets (Datasets 1-7) included comparable numbers of males ($n = 134$) and females ($n = 133$); the overall sex distribution did not deviate from 1:1 ($\chi^2(1) = 0.00$, $p = .95$), nor did it differ across datasets (7 cohorts; $\chi^2(6) = 7.41$, $p = .28$).

Reporting summary

Further information on research design is available in the Nature Portfolio Reporting Summary linked to this article.

Data availability

The corticospinal fMRI time-series data generated in this study have been deposited in Zenodo under the identifier https://doi.org/10.5281/zenodo.15469454. All raw data underlying the figures and extended data are provided in the accompanying Source Data file, which reproduces all plots in the manuscript. The DICOM imaging data are available under controlled access due to participant privacy and applicable data-protection regulations. Qualified researchers may request de-identified DICOMs for research, non-commercial use by (i) providing evidence of institutional ethics approval covering the proposed use, and (ii) signing a Data Use Agreement that prohibits re-identification, redistribution, and use beyond the approved purpose. Access requests should be submitted to Prof. Yazhuo Kong (kongyz@psych.ac.cn); requests will be reviewed and responded to within 15 working days. Source data are in this paper.

Code availability

All custom scripts and software components used for data processing, analysis, and generation of the main result are publicly available in the Zenodo at https://doi.org/10.5281/zenodo.15469454. When used in conjunction with the archived datasets, these scripts enable full reproduction of the study's principal figures and corticospinal-mapping results. The workflow for extraction of the RPN-signature[8] follows the procedure detailed by Spisak et al. and is available online at https://doi.org/10.1038/s41467-019-13785-z.

References

1. Kuehn, B. Chronic pain prevalence. *JAMA* **320**, 1632–1632 (2018).
2. Kohoutová, L. et al. Individual variability in brain representations of pain. *Nat. Neurosci.* **25**, 749–759 (2022).
3. Kehlet, H., Jensen, T. S. & Woolf, C. J. Persistent postsurgical pain: risk factors and prevention. *Lancet* **367**, 1618–1625 (2006).
4. Wager, T. D. et al. An fMRI-based neurologic signature of physical pain. *N. Engl. J. Med.* **368**, 1388–1397 (2013).
5. Rogachov, A. et al. Regional brain signal variability: a novel indicator of pain sensitivity and coping. *Pain* **157**, 2483–2492 (2016).
6. Zhang, R. et al. A neurofunctional signature of affective arousal generalizes across valence domains and distinguishes subjective experience from autonomic reactivity. *Nat. Commun.* **16**, 6492 (2025).
7. Tavor, I. et al. Task-free MRI predicts individual differences in brain activity during task performance. *Science* **352**, 216–220 (2016).
8. Spisak, T. et al. Pain-free resting-state functional brain connectivity predicts individual pain sensitivity. *Nat. Commun.* **11**, 187 (2020).
9. Lee, J. J. et al. A neuroimaging biomarker for sustained experimental and clinical pain. *Nat. Med.* **27**, 174–182 (2021).
10. Barry, R. L., Smith, S. A., Dula, A. N. & Gore, J. C. Resting state functional connectivity in the human spinal cord. *ELife* **3**, e02812 (2014).
11. Vahdat, S. et al. Resting-state brain and spinal cord networks in humans are functionally integrated. *PLOS Biol.* **18**, e3000789 (2020).
12. Vahdat, S. et al. Simultaneous brain-cervical cord fMRI reveals intrinsic spinal cord plasticity during motor sequence learning. *PLoS Biol.* **13**, e1002186 (2015).
13. Oliva, V., Hartley-Davies, R., Moran, R., Pickering, A. E. & Brooks, J. C. W. Simultaneous brain, brainstem, and spinal cord pharmacological-fMRI reveals involvement of an endogenous opioid network in attentional analgesia. *ELife* **11**, e71877 (2022).

14. Ioachim, G. et al. Altered Pain in the Brainstem and Spinal Cord of Fibromyalgia Patients During the Anticipation and Experience of Experimental Pain. *Front. Neurol.* **13**, 862976 (2022).
15. Tinnermann, A., Geuter, S., Sprenger, C., Finsterbusch, J. & Büchel, C. Interactions between brain and spinal cord mediate value effects in nocebo hyperalgesia. *Science* **358**, 105–108 (2017).
16. Finsterbusch, J., Eippert, F. & Büchel, C. Single, slice-specific z-shim gradient pulses improve T2*-weighted imaging of the spinal cord. *NeuroImage* **59**, 2307–2315 (2012).
17. Islam, H., Law, C. S. W., Weber, K. A., Mackey, S. C. & Glover, G. H. Dynamic per slice shimming for simultaneous brain and spinal cord fMRI. *Magn. Reson. Med.* **81**, 825–838 (2019).
18. Eippert, F., Kong, Y., Jenkinson, M., Tracey, I. & Brooks, J. C. W. Denoising spinal cord fMRI data: Approaches to acquisition and analysis. *Neuroimage* **154**, 255–266 (2017).
19. Fratini, M., Moraschi, M., Maraviglia, B. & Giove, F. On the impact of physiological noise in spinal cord functional MRI. *J. Magn. Reson. Imaging* **40**, 770–777 (2014).
20. De Leener, B. et al. PAM50: Unbiased multimodal template of the brainstem and spinal cord aligned with the ICBM152 space. *Neuroimage* **165**, 170–179 (2018).
21. Wilm, B. J. et al. Reduced field-of-view MRI using outer volume suppression for spinal cord diffusion imaging. *Magn. Reson. Med.* **57**, 625–630 (2007).
22. Lavaud, S., Bichara, C., D'Andola, M., Yeh, S.-H. & Takeoka, A. Two inhibitory neuronal classes govern acquisition and recall of spinal sensorimotor adaptation. *Science* **384**, 194–201 (2024).
23. Sharif-Naeini, R. & Basbaum, A. I. Targeting Pain Where It Resides … In the Brain. *Sci. Transl. Med.* **3**, 65ps61–65ps61 (2011).
24. Denk, F., McMahon, S. B. & Tracey, I. Pain vulnerability: a neurobiological perspective. *Nat. Neurosci.* **17**, 192–200 (2014).
25. Dapunt, U. et al. Quantitative sensory testing in physically active individuals and patients who underwent multidisciplinary pain therapy in the longitudinal course. *J. Pain. Res.* **11**, 2323–2330 (2018).
26. Arant, K. R., Katz, J. N. & Neogi, T. Quantitative sensory testing: identifying pain characteristics in patients with osteoarthritis. *Osteoarthr. Cartil.* **30**, 17–31 (2022).
27. Yarnitsky, D., Granot, M., Nahman-Averbuch, H., Khamaisi, M. & Granovsky, Y. Conditioned pain modulation predicts duloxetine efficacy in painful diabetic neuropathy. *Pain* **153**, 1193–1198 (2012).
28. Pan, L. H. et al. Pain sensitivities predict prophylactic treatment outcomes of flunarizine in chronic migraine patients: A prospective study. *Cephalalgia* **42**, 899–909 (2022).
29. Lee, M. C. et al. Human Labor Pain Is Influenced by the Voltage-Gated Potassium Channel K(V)6.4 Subunit. *Cell Rep.* **32**, 107941 (2020).
30. Mogil, J. S. et al. Melanocortin-1 receptor gene variants affect pain and μ-opioid analgesia in mice and humans. *J. Med. Genet.* **42**, 583–587 (2005).
31. Sacharczuk, M. et al. Distinct susceptibility to inoculated melanoma and sensitivity to cancer pain in mouse lines with high and low sensitivity to stress. *J. Environ. Pathol. Toxicol. Oncol.* **31**, 167–177 (2012).
32. Lindquist, M. A., Xu, Y., Nebel, M. B. & Caffo, B. S. Evaluating dynamic bivariate correlations in resting-state fMRI: a comparison study and a new approach. *Neuroimage* **101**, 531–546 (2014).
33. Zambreanu, L., Wise, R. G., Brooks, J. C. W., Iannetti, G. D. & Tracey, I. A role for the brainstem in central sensitisation in humans. Evidence from functional magnetic resonance imaging. *Pain* **114**, 397–407 (2005).
34. Roy, M., Piché, M., Chen, J. I., Peretz, I. & Rainville, P. Cerebral and spinal modulation of pain by emotions. *Proc. Natl. Acad. Sci. USA* **106**, 20900–20905 (2009).
35. Lopes, P. S. S., Campos, A. C. P., Fonoff, E. T., Britto, L. R. G. & Pagano, R. L. Motor cortex and pain control: exploring the descending relay analgesic pathways and spinal nociceptive neurons in healthy conscious rats. *Behav. Brain Funct.* **15**, 5 (2019).
36. Huynh, V. et al. Descending pain modulatory efficiency in healthy subjects is related to structure and resting connectivity of brain regions. *Neuroimage* **247**, 118742 (2022).
37. Maixner, W., Fillingim, R. B., Williams, D. A., Smith, S. B. & Slade, G. D. Overlapping Chronic Pain Conditions: Implications for Diagnosis and Classification. *J. Pain.* **17**, T93–t107 (2016).
38. Tanguay-Sabourin, C. et al. A prognostic risk score for development and spread of chronic pain. *Nat. Med.* **29**, 1821–1831 (2023).
39. Khoury, S. et al. Genome-wide analysis identifies impaired axonogenesis in chronic overlapping pain conditions. *Brain* **145**, 1111–1123 (2022).
40. Apkarian, A. V., Baliki, M. N. & Geha, P. Y. Towards a theory of chronic pain. *Prog. Neurobiol.* **87**, 81–97 (2009).
41. Marek, S. et al. Reproducible brain-wide association studies require thousands of individuals. *Nature* **603**, 654–660 (2022).
42. Wu, X. et al. Sex difference in trait empathy is encoded in the human anterior insula. *Cereb. Cortex* **33**, 5055–5065 (2023).
43. Zhang, H. et al. The role of negative emotions in sex differences in pain sensitivity. *Neuroimage* **245**, 118685 (2021).
44. Lefaucheur, J. P. et al. Evidence-based guidelines on the therapeutic use of repetitive transcranial magnetic stimulation (rTMS): An update (2014-2018). *Clin. Neurophysiol.* **131**, 474–528 (2020).
45. D'Mello, R. & Dickenson, A. H. Spinal cord mechanisms of pain. *Br. J. Anaesth.* **101**, 8–16 (2008).
46. Timme, N. M. & Lapish, C. A tutorial for information theory in neuroscience. *eNeuro* **5**, https://doi.org/10.1523/eneuro.0052-18.2018 (2018).
47. Noble, S., Scheinost, D. & Constable, R. T. A decade of test-retest reliability of functional connectivity: A systematic review and meta-analysis. *Neuroimage* **203**, 116157 (2019).
48. Harris, G. & Rollman, G. B. The validity of experimental pain measures. *Pain* **17**, 369–376 (1983).
49. Chen, Q. & Heinricher, M. M. Descending Control Mechanisms and Chronic Pain. *Curr. Rheumatol. Rep.* **21**, 13 (2019).
50. Thiebaut de Schotten, M. & Forkel, S. J. The emergent properties of the connected brain. *Science* **378**, 505–510 (2022).
51. Pessoa, L. The Entangled Brain. *J. Cogn. Neurosci.* **35**, 349–360 (2023).
52. Woo, C. W., Chang, L. J., Lindquist, M. A. & Wager, T. D. Building better biomarkers: brain models in translational neuroimaging. *Nat. Neurosci.* **20**, 365–377 (2017).
53. Innocenti, G. M. et al. The functional characterization of callosal connections. *Prog. Neurobiol.* **208**, 102186 (2022).
54. Finn, E. S. et al. Functional connectome fingerprinting: identifying individuals using patterns of brain connectivity. *Nat. Neurosci.* **18**, 1664–1671 (2015).
55. Gan, Z. et al. Layer-specific pain relief pathways originating from primary motor cortex. *Science* **378**, 1336–1343 (2022).
56. Kuner, R. & Kuner, T. Cellular circuits in the brain and their modulation in acute and chronic pain. *Physiol. Rev.* **101**, 213–258 (2021).
57. Kolesnikov, Y., El-Maarouf, A., Rutishauser, U. & Pasternak, G. Reorganization of dorsal root ganglion neurons following chronic sciatic nerve constriction injury: correlation with morphine and lidocaine analgesia. *Eur. J. Pharm.* **568**, 124–133 (2007).
58. Frot, M., Magnin, M., Mauguière, F. & Garcia-Larrea, L. Cortical representation of pain in primary sensory-motor areas (S1/M1)–a study using intracortical recordings in humans. *Hum. Brain Mapp.* **34**, 2655–2668 (2013).
59. Eippert, F., Finsterbusch, J., Bingel, U. & Büchel, C. Direct evidence for spinal cord involvement in placebo analgesia. *Science* **326**, 404 (2009).

60. Lad, S. P. et al. Racial disparities in outcomes after spinal cord injury. *J. Neurotrauma* **30**, 492–497 (2013).
61. Riddle, J. et al. A guide for concurrent TMS-fMRI to investigate functional brain networks. *Front Hum. Neurosci.* **16**, 1050605 (2022).
62. ElSayed, N. A. et al. 2. Classification and Diagnosis of Diabetes: Standards of Care in Diabetes-2023. *Diabetes Care* **46**, S19–s40 (2023).
63. Dworkin, R. H. et al. Development and initial validation of an expanded and revised version of the Short-form McGill Pain Questionnaire (SF-MPQ-2). *Pain* **144**, 35–42 (2009).
64. Finnerup, N. B. et al. Neuropathic pain: an updated grading system for research and clinical practice. *Pain* **157**, 1599–1606 (2016).
65. Rolke, R. et al. Quantitative sensory testing in the German Research Network on Neuropathic Pain (DFNS): standardized protocol and reference values. *Pain* **123**, 231–243 (2006).
66. Wasner, G. L. & Brock, J. A. Determinants of thermal pain thresholds in normal subjects. *Clin. Neurophysiol.* **119**, 2389–2395 (2008).
67. Marcuzzi, A., Wrigley, P. J., Dean, C. M., Adams, R. & Hush, J. M. The long-term reliability of static and dynamic quantitative sensory testing in healthy individuals. *Pain* **158**, 1217–1223 (2017).
68. Amir, C. et al. Test-Retest Reliability of an Adaptive Thermal Pain Calibration Procedure in Healthy Volunteers. *J. Pain.* **23**, 1543–1555 (2022).
69. Fisch, L. et al. deepbet: Fast brain extraction of T1-weighted MRI using convolutional neural networks. *Comput. Biol. Med.* **179**, 108845 (2024).
70. Urchs, S. et al. MIST: A multi-resolution parcellation of functional brain networks. *MNI Open Res.* **1**, 3 (2019).
71. Ezra, M., Faull, O. K., Jbabdi, S. & Pattinson, K. T. Connectivity-based segmentation of the periaqueductal gray matter in human with brainstem optimized diffusion MRI. *Hum. Brain Mapp.* **36**, 3459–3471 (2015).
72. Fonov, V. S. et al. Framework for integrated MRI average of the spinal cord white and gray matter: the MNI-Poly-AMU template. *Neuroimage* **102**, 817–827 (2014).
73. Xu, H. et al. Impact of global signal regression on characterizing dynamic functional connectivity and brain states. *Neuroimage* **173**, 127–145 (2018).
74. Marrelec, G. et al. Partial correlation for functional brain interactivity investigation in functional MRI. *Neuroimage* **32**, 228–237 (2006).
75. Yeo, B. T. et al. The organization of the human cerebral cortex estimated by intrinsic functional connectivity. *J. Neurophysiol.* **106**, 1125–1165 (2011).

Acknowledgements

We are grateful to all colleagues and clinical staff who contributed to this project. This research was supported by the National Natural Science Foundation of China (No. 82441056 to Y.K.; No. 82071883 and No. 82371937 to J.-Q.Z.), the National Key R&D Program of China (No. 2022YFC3500603 to Y.K. and J.-X.L), the Beijing Natural Science Foundation (No. IS23108 to Y.K.).

Author contributions

X.L., L.Z., and Y.K. designed the study; X.L., X.Z., J.-Y.Z., and Y.K. performed data analysis; L.G., B.N., J.-Q. Z., Z.W., M.S., Z.J., Y.H., Y.L., and Y.D. performed data acquisition; X.L. and X.Z. drew figures; The original draft was written by X.L. with Y.K., L.G., B.N., J.-Q. Z., L.Z., X.Z., L.H., M.Z., J.L., L.C., J.B., T.W., and I.T. reviewing and editing the draft. All authors reviewed and accepted the final draft of the manuscript.

Competing interests

The authors declare no competing interests.

Additional information

Supplementary information The online version contains supplementary material available at https://doi.org/10.1038/s41467-025-67132-6.

Correspondence and requests for materials should be addressed to Ling-Fei Guo, Bing Ni, Jiu-Quan Zhang, Ya-Ou Liu or Ya-Zhuo Kong.

Peer review information *Nature Communications* thanks the anonymous reviewers for their contribution to the peer review of this work. A peer review file is available.